J. Fluid Mech. (2015), *vol.* 766, *pp.* 436–467.
doi:10.1017/jfm.2015.10

Thermocapillary migration and interaction of drops: two non-merging drops in an aligned arrangement

Zhaohua Yin[1,†] **and Qiaohong Li**[1,2]

[1]National Microgravity Laboratory, Institute of Mechanics, Chinese Academy of Sciences, Beijing 100190, PR China

[2]Educational Equipment R&D Center, Ministry of Education, Beijing, PR China

(Received 23 February 2014; revised 5 September 2014; accepted 6 January 2015; first published online 4 February 2015)

A numerical study on the interaction of two spherical drops in thermocapillary migration in microgravity is presented. Unequal drop sizes in the axisymmetric model lead to strong drop interaction if the leading drop is smaller. The effect of the ratio of the two drop radii, their initial distance apart, and non-dimensional numbers on the interaction is studied in the case of non-merging drops in detail. The Marangoni number adopted in this paper is fairly large (around 100) so as to reveal the phenomena of real flows. As a result, the heat wake behind the leading drop plays an important role in drop interaction, and obviously different final drop distances and transient migration processes are observed for various sets of non-dimensional numbers. The influence of drop deformation on drop interaction is also investigated for relatively large capillary number (up to 0.2). Finally, some simulations are performed to explain the phenomena of drop interaction in previous experiments, and some suggestions for future experiments are also provided.

Key words: drops and bubbles, multiphase flow, thermocapillarity

1. Introduction

The motion of drops and bubbles is a frequently observed physical phenomenon in nature, e.g. movement of raindrops and vapour bubbles in boiling water. It is a classical problem in fluid mechanics, and its study has great scientific value. Moreover, droplets and bubbles widely exist in various production processes, e.g. fuel droplets in the combustion chambers of power devices, bubbles in crystal growth, and liquid drops and bubbles in the chemical process of aggregation and extraction. Hence, the study of the behaviour of bubbles or droplets has a strong engineering background.

When gravity cannot be neglected, droplets or bubbles migrate due to the buoyancy caused by density differences. In the microgravity environment, the buoyancy effect disappears, and some other forces must be induced to drive droplets. A common practice is making the mother liquid have non-uniform temperature. Since the interfacial tension decreases with increasing temperature, the liquid near the interface

† Email address for correspondence: zhaohua.yin@gmail.com

is dragged towards the cold end from the hot end, the viscous force then drives the mother liquid around the drop/bubble towards the colder region, and the counterforce pushes the drop/bubble towards the hotter region. This phenomenon is termed thermocapillary migration.

The earliest studies of thermocapillary migration were performed by Young, Goldstein & Block (1959, the so-called YGB theory). Their linear model dealing with this problem adopted the Stokes equation, and the steady Marangoni migration velocity was derived:

$$v_{YGB} = \frac{2U}{(2+3\alpha)\,(2+\lambda)}, \tag{1.1}$$

where

$$\alpha = \mu_1/\mu_2, \quad \lambda = k_1/k_2. \tag{1.2a,b}$$

In this paper, symbols with subscript 1 represent physical quantities of the mother liquid, and those with subscript 2 the physical quantities of the drop; μ is the kinematic viscosity, and k the coefficient of thermal conductivity. The reference speed U is defined using the balance of the thermocapillary force and viscous force:

$$U = |\sigma_T|\,|\nabla T_\infty|\,R/\mu_1, \tag{1.3}$$

where σ_T is the changing rate of interface tension with temperature ∇T_∞ the background temperature gradient of the mother liquid, and R the radius of the droplet.

Before the phenomena of two-drop migration are discussed, it is necessary to review the main previous studies of a single drop. Traditionally, the density (ρ), μ, k, and the specific heat (c_p) are assumed to be constants. Hence, seven non-dimensional numbers are considered in the one-drop system:

$$\alpha,\ \lambda,\ Ma = UR/\kappa_1, \quad Re = UR\rho_1/\mu_1, \quad Ca = \mu_1 U/\sigma_0, \quad \xi = \rho_2/\rho_1, \quad \gamma = c_{p2}/c_{p1}. \tag{1.4a–e}$$

Here, $\kappa = k/\rho c_p$ is the thermal diffusivity, σ_0 the interface tension at a reference temperature T_0, and Ma, Re and Ca are the Marangoni, Reynolds and capillary numbers, respectively.

Since the YGB theory was published, there have been many studies on this problem using theoretical, experimental and numerical tools (see Balasubramaniam & Chai 1987; Chen & Lee 1992; Treuner *et al.* 1996; Haj-Hariri, Shi & Borhan 1997; Welch 1998; Wozniak *et al.* 2001; Sun & Hu 2002, 2003; Nas, Muradoglu & Tryggvason 2006; Borcia & Bestehorn 2007; Liu, Zhang & Valocchi 2012; Liu *et al.* 2013). Most early findings have been summarized and discussed in the review book by Subramanian & Balasubramaniam (2001); see also Subramanian, Balasubramaniam & Wozniak (2002). Due to the fast development of supercomputers, it is possible to perform more intensive numerical studies on this issue. In particular, Yin *et al.* (2008) performed a thorough study on how all non-dimensional numbers influence the migration process of non-deformable drops. The analytical study of the deformable drop was first carried out by Haj-Hariri, Nadim & Borhan (1990). With numerical simulations, the topological structure of the velocity and temperature field for the deformed drop was studied by Zhao *et al.* (2011). The corresponding transient behaviour was studied by Chang, Yin & Hu (2011), showing that changing the density ratio (ξ) leads to totally different drop shapes.

Most investigations have so far concentrated on the system of a Fluorinert FC-75 drop and a silicone oil continuous phase. For large Ma (>100), numerical simulation is more challenging since the temperature boundary layer is very thin and the

migration distance is very long (Brady, Herrmann & Lopez 2011). With the help of a solver of the dynamic computing zone, the results of experiments in space (Hadland *et al.* 1999) have been well explained by numerical simulations (Yin *et al.* 2012). With the asymptotic method, Wu & Hu (2013) argued that there will not be a stable migration velocity for large Ma. Note that this theoretical result is consistent with the numerical simulations since there is a dramatic increase in computed stable drop velocities for $Ma > 200$ (see figure 15 of Yin *et al.* 2012). Further theoretical studies were also carried out with a Stokes model (Choudhuri & Raja Sekhar 2013; Lee & Keh 2013), and the influence of various non-dimensional numbers was studied.

In practice, there are normally two or more drops existing in a mother liquid, so it is very important to study the interaction between them. The first theoretical study on two drops was carried out by Anderson (1985), and he found that the interaction caused by thermocapillary effects is much weaker than that caused by buoyancy. Later, a two-drop axisymmetric model was adopted by Keh & Chen (1990) and Keh & Chen (1992). The axisymmetric thermocapillary-driven motion of a pair of unequal spherical drops in near contact and subject to an ambient temperature gradient was investigated for the case of non-conducting drops by Loewenberg & Davis (1993). They studied touching drops in point contact (relative motion for the nearly touching drops resulting from the contact force balanced by a lubrication resistance). Results for the pairwise migration velocity, contact force, and the relative and individual drop velocities were presented for many size ratios and a wide range of viscosity ratios (also, asymptotic formulae were derived for small size ratios). The interaction between two deformable drops was investigated by Zhou & Davis (1996).

Based on the space experiments (Balasubramanian *et al.* 1996), an asymptotic analysis was applied to two bubbles at large Re and Ma (Balasubramanian & Subramanian 1999), and it was concluded that the thermal wake of the leading drop slows down the trailing drop. Lavrenteva & Nir (2003) considered the axisymmetric motion and related thermal wake interaction of two drops in a viscous fluid under the combined effect of gravity and thermocapillarity ($Re < 1$, $Ma > 1$, $Pr \gg 1$, where $Pr := Ma/Re$ is the Prandtl number). Without an imposed initial temperature gradient in the external liquid, the analysis was focused on the case of 'spontaneous' thermocapillary motion, i.e. Marangoni effects induced on the trailing droplet by the thermal wake originated from a leading rising drop moving under the effect of buoyancy forces. They found that thermal boundary layers are present along the interfaces at large Marangoni number, and thermal wakes are formed downstream of the drops. The thermal wake behind the leading drop was proven to influence significantly the temperature distribution on the surface of the trailing drop. They also found that the induced change in the speed of the trailing drop becomes comparable in magnitude with its (buoyancy) speed when isolated even for large separation distance between the drops where the hydrodynamic interaction is negligible, and that in the extreme case of very large Marangoni effect the direction of the trailing drop can be reversed. In a subsequent study (Frolovskaya, Nir & Lavrenteva 2006), the above results were refined by analysing in detail how the induced Marangoni flow results in the change of the flow pattern, the velocity of both particles, and the equilibrium separation distance (see also Leshansky & Nir 2001). With the front-tracking scheme, two- and three-dimensional multi-drop problems were studied by Nas & Tryggvason (2003), Nas *et al.* (2006) and Yin *et al.* (2011). It was found that two drops with the same radius tend to move away from each other, and there is weaker interaction between drops thereafter (Yin *et al.* 2011). In a study with the volume of fluid method, Lappa (2005) assessed the role played by thermal wake effects in complex multi-droplet configurations for both small and large values of the Prandtl number.

However, most past studies on the interaction of droplets in the course of their Marangoni migration were performed under the assumption of creeping flow (vanishing *Re* and *Ma*, see Subramanian & Balasubramaniam 2001). For real flows, it is expected that, when the values of the Marangoni number are relatively large, thin thermal boundary layers will develop along the liquid–liquid interface, leading to the formation of well-defined thermal wakes at the rear of a moving drop. In principle, the thermal wake field of a leading drop could wrap around a trailing drop and have a significant impact on its motion. The main focus of this paper is to further explore this kind of strong drop interaction.

This research considers the axisymmetric model, for convenient comparison with the planned space experiment in China. Previous space experiments are not very informative because only the temperature at a few locations could be measured, while the temperature field has the most important influence on thermocapillary migration. With the axisymmetric assumption and digital holographic interferometry (e.g. see Schedin 2006), it is possible to record the full temperature field without the need for a large amount of equipment to be shipped for space experiments.

This paper is arranged as follows: the governing equations and numerical methods are introduced in § 2, and a benchmark simulation is described in § 3. Sections 4 and 5 discuss how the ratio of the radii of the two drops and their initial distance affect the interaction, § 6 discusses the influence of non-dimensional numbers for non-deformable drops, and § 7 briefly discusses the case of deformable drops. Some comparisons between our simulations and previous space experiments are made in § 8, and our results and those of 'creeping flows' are compared in § 9. The conclusions are presented in § 10.

2. The physical model and numerical solver

In this study, the axisymmetric model is adopted to perform high-resolution simulations. Two drops are surrounded by the bulk fluid in a cylinder $\Omega = [0, r_1] \times [z_0, z_1]$. The direction of the temperature gradient is along the z-axis (figure 1). The centreline of the two drops is $r = 0$. S is the distance between the drop centres, and S_0 the initial distance. We use S_F to denote the distance at the final steady state. (For an isolated drop, the final state means that a steady migration velocity is reached. For the two-drop system, the final state is reached when both drops have identical velocities.) The trailing drop is at a relatively low temperature, and the leading drop is in the hotter region. We select the radius of the trailing drop as the reference length (R), and Λ is the radius ratio of the leading drop to the trailing drop. $G = S - R - R\Lambda$ is the gap between the interfaces of the two drops, and G_F the gap at the final steady state. It is well-known in this field that a larger drop leads to a larger migration velocity, so there will be weaker interaction for the case of $\Lambda \geqslant 1$ because S becomes larger after the simulation is started. Hence, we set $\Lambda < 1$ throughout this paper.

The governing equations for the entire domain can be written as

$$\nabla \cdot \boldsymbol{u} = 0, \tag{2.1}$$

$$\frac{\partial(\rho \boldsymbol{u})}{\partial t} + \nabla \cdot (\rho \boldsymbol{u}\boldsymbol{u}) = -\nabla p + \nabla \cdot (\mu(\nabla \boldsymbol{u} + \nabla^{\mathrm{T}} \boldsymbol{u})) + \boldsymbol{F}_\sigma, \tag{2.2}$$

$$\rho C_p \left(\frac{\partial T}{\partial t} + \boldsymbol{u} \cdot \nabla T \right) = \nabla \cdot (k \nabla T). \tag{2.3}$$

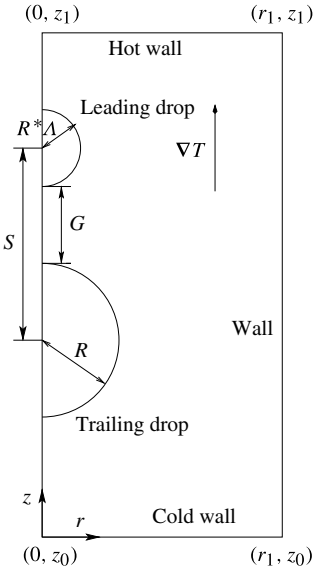

FIGURE 1. The schematic diagram for the Marangoni migration.

Here, $\boldsymbol{u} = (u, w)$ is the velocity vector, and $\boldsymbol{F}_\sigma$ is the body force term produced by the interfacial tension

$$\boldsymbol{F}_\sigma = \int_B \delta(\boldsymbol{x} - \boldsymbol{x}_f) \left(\sigma \zeta \boldsymbol{n} + \frac{\partial \sigma}{\partial s} \boldsymbol{\tau} \right) \mathrm{d}s, \tag{2.4}$$

where $\boldsymbol{x} = (r, z)$ is the space vector, $\boldsymbol{x}_f = (r_f, z_f)$ the position of cell f on the interface B, δ a delta function, σ the interfacial tension, ζ the sum of two principal curvatures of the interface, and s the natural coordinate along the interface; $\boldsymbol{n} = (n_r, n_z)$ and $\boldsymbol{\tau}$ denote the normal and tangential unit vectors of the interface, respectively. Note that, in this paper and most related research in this field, σ usually takes the following form:

$$\sigma(T) = \sigma_0 - \sigma_T (T - T_0). \tag{2.5}$$

Hence, when T is high enough, the simulation has to be stopped to avoid $\sigma(T) < 0$.

The non-dimensional quantities are defined as

$$\left.\begin{array}{c} \bar{\boldsymbol{u}} = (\bar{u}, \bar{w}) = \boldsymbol{u}/U, \quad \bar{\boldsymbol{x}} = (\bar{r}, \bar{z}) = \boldsymbol{x}/R, \quad \bar{t} = t \,/ (R/U), \quad \bar{p} = p/(\rho_1 U^2), \\ \bar{T} = T/(|\nabla T| R), \quad \bar{\rho} = \rho/\rho_1, \quad \bar{\mu} = \mu/\mu_1, \quad \bar{k} = k/k_1, \\ \bar{C}_p = C_p/C_{p1}, \quad \bar{\boldsymbol{F}}_\sigma = \boldsymbol{F}_\sigma R/(\rho_1 U^2), \quad \bar{S} = S/R. \quad \bar{G} = G/R. \end{array}\right\} \tag{2.6}$$

Thus, we have the non-dimensional equations

$$\nabla \cdot \bar{\boldsymbol{u}} = 0, \tag{2.7}$$

$$\frac{\partial(\bar{\rho}\bar{\boldsymbol{u}})}{\partial \bar{t}} + \nabla \cdot (\bar{\rho}\bar{\boldsymbol{u}}\bar{\boldsymbol{u}}) = -\nabla \bar{p} + \frac{1}{Re} \nabla \cdot (\bar{\mu}(\nabla \bar{\boldsymbol{u}} + \nabla^{\mathrm{T}} \bar{\boldsymbol{u}})) + \bar{\boldsymbol{F}}_\sigma, \tag{2.8}$$

$$\bar{\rho} \bar{C}_p \left(\frac{\partial \bar{T}}{\partial t} + \bar{\boldsymbol{u}} \cdot \nabla \bar{T} \right) = \frac{1}{Ma} \nabla \cdot (\bar{k} \nabla \bar{T}). \tag{2.9}$$

The boundary conditions on the solid walls are

$$\left.\begin{aligned} \bar{u}|_{\bar{r}=\bar{r}_1} = \bar{u}|_{\bar{z}=\bar{z}_0,\bar{z}_1} = 0, \\ \bar{w}|_{\bar{r}=\bar{r}_1} = \bar{w}|_{\bar{z}=\bar{z}_0,\bar{z}_1} = 0, \\ \bar{T}|_{\bar{r}=\bar{r}_1} = \bar{T}_0 + \bar{z}, \\ \bar{T}|_{\bar{z}=\bar{z}_0} = \bar{T}_0 + \bar{z}_0, \\ \bar{T}|_{\bar{z}=\bar{z}_1} = \bar{T}_0 + \bar{z}_1. \end{aligned}\right\} \tag{2.10}$$

The boundary conditions on the symmetry axis are

$$\bar{u}|_{\bar{r}=0} = 0, \quad \left.\frac{\partial \bar{w}}{\partial \bar{r}}\right|_{\bar{r}=0} = 0, \quad \left.\frac{\partial \bar{T}}{\partial \bar{r}}\right|_{\bar{r}=0} = 0. \tag{2.11a–c}$$

The initial conditions are

$$\bar{u}|_{\bar{t}=0} = \bar{w}|_{\bar{t}=0} = 0, \quad \bar{T}|_{\bar{t}=0} = \bar{T}_0 + \bar{z}. \tag{2.12a,b}$$

The non-dimensional form of the interfacial tension is

$$\bar{\sigma} = \frac{\sigma_0 + \sigma_T(T - T_0)}{\rho_1 U^2 R} = \frac{1}{ReCa} - \frac{1}{Re}(\bar{T} - \bar{T}_0). \tag{2.13}$$

In this paper, T_0 is the temperature at the initial centre of the trailing drop (where $\bar{x} = (0, 3)$). Therefore, to avoid the non-physical negative σ in our calculation, the limitation for the non-dimensional migration distance of the leading drop is

$$M_l = \frac{1}{Ca} - \bar{S} - \Lambda. \tag{2.14}$$

In the following, symbols without bars are adopted to indicate non-dimensional values. The front-tracking method is employed in our simulations (see Tryggvason *et al.* 2001; Yin *et al.* 2008), a dynamic zone is adopted to enlarge the effective computing domain (Yin *et al.* 2012), and a hybrid iterative scheme is adopted to accelerate the code (Li 2013).

Throughout this paper, unless specified, the computational domain is 4×20 with the resolution of 400×2000, and the time step is 0.0015. The exceptions are those simulations with small Λ (§ 5), small Ma (§ 6.1), and larger Ca (§ 7). All simulations are continued until T_F: when the relative velocity difference of two drops remains $<1\,\%$ for certain period (about two time units). The migration distance of the leading drop at $t = T_F$ is defined as M_F.

3. A benchmark problem

In this section, we adopt the physical parameters of a Fluorinert FC-75 drop and a continuous phase with DC-200 silicone oil of nominal viscosity 10 cSt (Hadland *et al.* 1999). For the benchmark problem in this section, the non-dimensional parameters are: $Pr = 83.3$, $\alpha = 0.14$, $\lambda = 0.47$, $\xi = 1.89$, $\gamma = 0.69$, $Ca = 0.04$, $Ma = 100$, $\Lambda = 0.5$, and $S_0 = 2.5$.

An isolated drop with a fairly large Ma experiences an increase–decrease process before it reaches its final steady velocity (V_F) (e.g. see the curves with 'plus'

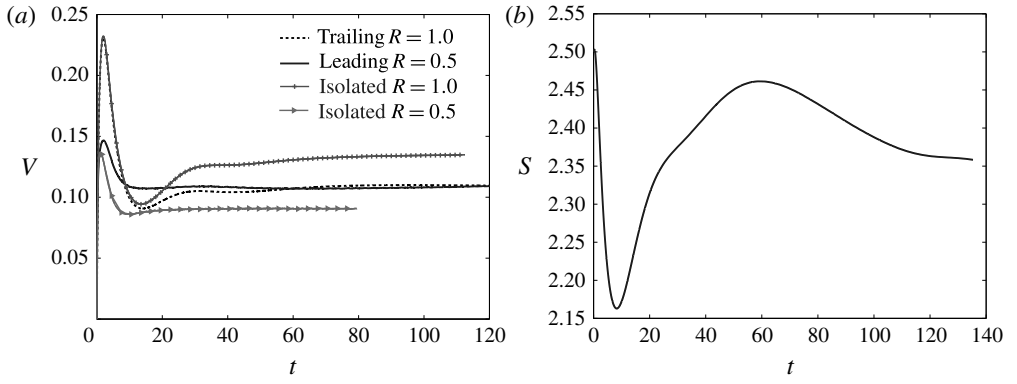

FIGURE 2. Time evolution of drop velocities V (a) and distance between centres S (b) for the benchmark simulation. $Re = 1.2$, $\alpha = 0.14$, $\lambda = 0.47$, $\xi = 1.89$, $\gamma = 0.69$, $Ca = 0.04$, $Ma = 100$, $\Lambda = 0.5$ and $S_0 = 2.5$.

or triangle marks in figure 2a). When two drops migrate together, there is some difference in migration velocities. It is clear that the trailing drop starts with a rapid acceleration and deceleration, forming a sharp overshoot in velocity. By contrast, the leading drop has a much smaller overshoot, and eventually reaches the same velocity as the trailing drop (solid and dashed lines in figure 2a). The common speed of the coupled drops is slower than that of the bigger isolated drop (the '+' curve in figure 2a), but faster than that of the smaller isolated drop (the triangle-mark curve in figure 2a).

Figure 2(b) shows the time evolution of S. It decreases before $t = 9$ because the trailing drop has a much bigger acceleration, but becomes larger after $t = 9$ because the trailing drop becomes much slower after the overshoot. After an interaction process between the two drops, they reach the same velocity, and S becomes a constant.

In the Marangoni phenomenon, the velocity field surrounding the drop is not very strong because the effective Re is very low. That is, if the reference speed is defined as the maximal or average speed in the flow field instead of (1.3), Re is lower than 10. In fact, the variation in the temperature field is the most important factor in the interaction between two drops, and it is worth a thorough investigation. At the beginning of the simulation, isotherms of the whole flow field are straight (figure 3, $t = 0$), or there is fairly large temperature difference along the drop interfaces. This leads to a large driving force on the drops. When the drops move forwards, the isotherms wrap around the interfaces. After a while, the temperature differences of both drops are smaller than those at $t = 0$ (figure 3, $t = 15$), and drop velocities begin to decrease. Figure 4(b) clearly shows that scaled temperature distributions along the leading drop are almost the same after $t = 30$, and the drop velocity becomes stable. (Note that the scales of the y-axis in left-hand plots of figures 4, 10 and 13 are about twice those in right-hand panels (b).) On the other hand, the trailing drop becomes stable much more slowly (figure 4a). During $t \in [15, 60]$, there are still dramatic changes in the isotherms inside the trailing drop, and the cold region in the drop top becomes colder and colder compared with the mother liquid nearby. This change makes a stronger temperature boundary near the trailing drop, and leads to a larger temperature difference on the interface and to a larger drop velocity. The trailing drop does not reach its steady velocity until $t = 60$.

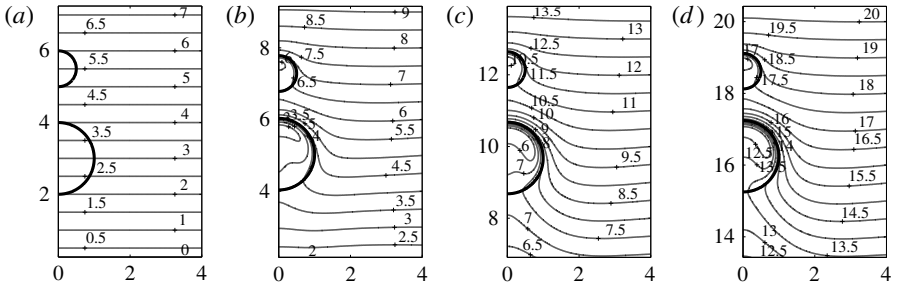

FIGURE 3. Temperature fields of the benchmark simulation at different times. $Re = 1.2$, $\alpha = 0.14$, $\lambda = 0.47$, $\xi = 1.89$, $\gamma = 0.69$, $Ca = 0.04$, $Ma = 100$, $\Lambda = 0.5$ and $S_0 = 2.5$. (*a*) $t = 0$; (*b*) $t = 15$; (*c*) $t = 60$; (*d*) $t = 120$.

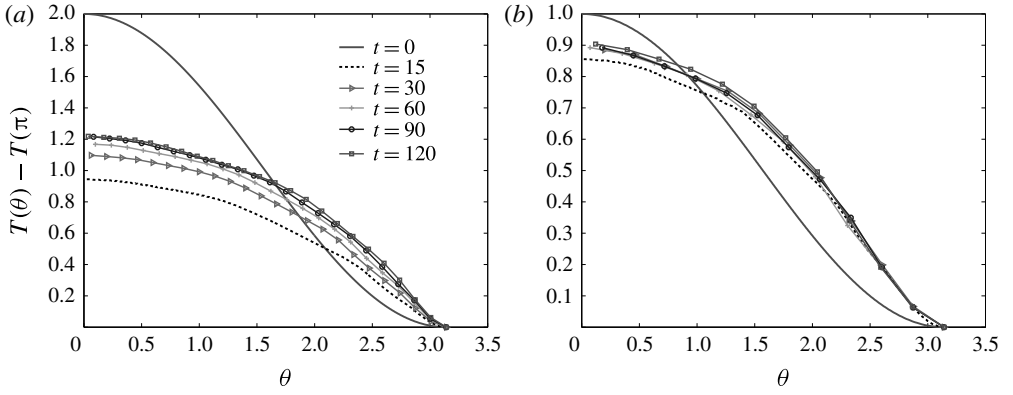

FIGURE 4. Scaled temperature distributions along the drop interfaces for the benchmark simulation. Throughout this paper, θ is defined as the angle from the interface to the drop centre. $\theta = 0$ corresponds to the top of the drop, and $\theta = \pi$ to the bottom of the drop. $Re = 1.2$, $\alpha = 0.14$, $\lambda = 0.47$, $\xi = 1.89$, $\gamma = 0.69$, $Ca = 0.04$, $Ma = 100$, $\Lambda = 0.5$ and $S_0 = 2.5$. (*a*) Trailing drop: $R = 1.0$; (*b*) leading drop: $R = 0.5$.

Figures 5(*a*) and 5(*c*) show temperature fields when two isolated drops migrate to their steady velocities. They clearly show that the isotherms accumulate around the drop front, where the temperature gradient along the z axis is very large. On the other hand, there is a long thermal wake behind the drop, where the temperature gradient along the z axis is very small. When two droplets migrate together (figure 5*b*), the thermal wake caused by the leading drop lowers the temperature gradient around the trailing drop, and the trailing drop moves more slowly than the isolated drop. On the other hand, the accumulated isotherms around the head of the trailing drop leads to a hotter rear stagnation point on the leading drop, so the leading drop moves faster than if isolated.

At the final steady states, isotherms between two droplets (figure 5*b*) are denser than those behind an isolated small drop (figure 5*a*), and sparser than those in front of an isolated large drop (figure 5*c*). This is much clearer in figure 6, where the temperature-difference curves related to the pair of drops (the solid and dashed lines) are between those of two isolated drops (the lines with '+' and triangle marks).

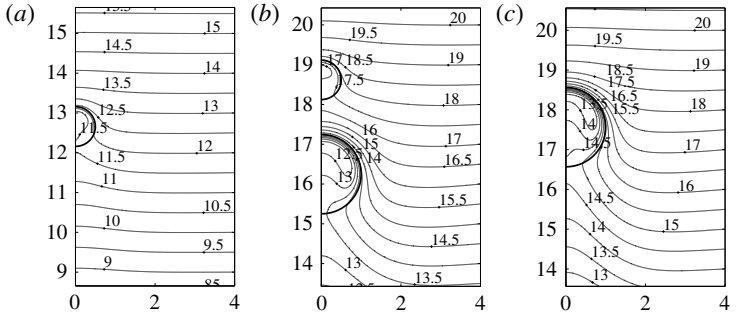

FIGURE 5. Temperature fields of the benchmark simulation and isolated droplets at the final states. $Re = 1.2$, $\alpha = 0.14$, $\lambda = 0.47$, $\xi = 1.89$, $\gamma = 0.69$, $Ca = 0.04$, $Ma = 100$, $\Lambda = 0.5$ and $S_0 = 2.5$. (*a*) Isolated drop $R = 0.5$; (*b*) two drops $R_1 = 1.0$, $R_2 = 0.5$; (*c*) isolated drop $R = 1.0$.

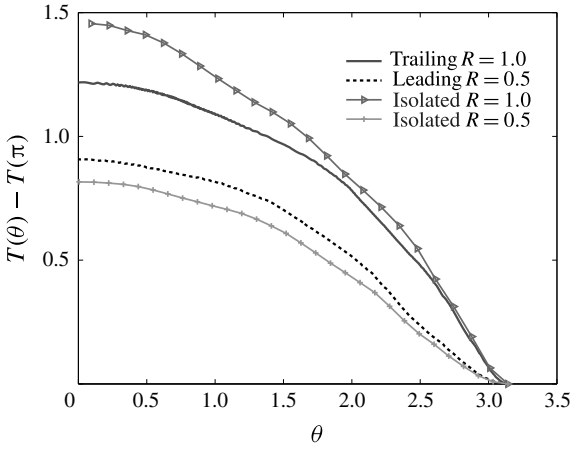

FIGURE 6. Scaled temperature distributions along the drop interfaces at the final states. $Re = 1.2$, $\alpha = 0.14$, $\lambda = 0.47$, $\xi = 1.89$, $\gamma = 0.69$, $Ca = 0.04$, $Ma = 100$, $\Lambda = 0.5$ and $S_0 = 2.5$.

Figure 2(*a*) also shows that the influence of the trailing drop on the leading drop takes effect much earlier than that of the leading drop on the trailing drop. To explain this phenomenon, we draw the temperature perturbation $(T(r, z, t) - T(r, z, 0))$ for the isolated droplet. At $t = 1.5$ (figure 7*a*), the disturbance from the front stagnation point ('stagnation point' is adopted here because the velocity is zero at the front/rear point of the drop in the reference frame moving with the drop, see e.g. figure 6(*b*) in Yin *et al.* (2008)) has already spread about $2R$ ahead, while that from the rear stagnation point has only spread about R behind. In other words, the disturbance spreads faster from the front part than the rear part of the drop. In the case of the two-drop system, this means that the influence of the trailing drop spreads faster than that of the leading drop at the beginning of the simulation. At $t = 15$ (figure 7*b*), the disturbance from both front and rear parts has spread about $2R$ away. So in the case of the two-drop system, the influence of the trailing drop is of the same importance as that of the leading drop at this stage.

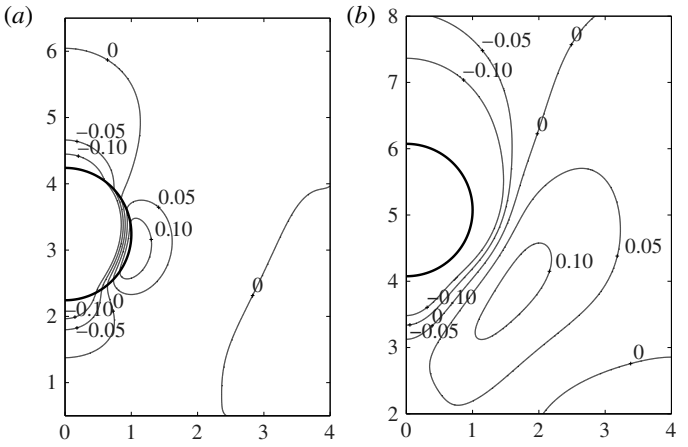

FIGURE 7. Temperature perturbation for the isolated droplet at different times. The isotherms labelled zero indicate the undisturbed region. $Re = 1.2$, $\alpha = 0.14$, $\lambda = 0.47$, $\xi = 1.89$, $\gamma = 0.69$, $Ca = 0.04$, $Ma = 100$, $\Lambda = 0.5$ and $S_0 = 2.5$. (*a*) $t = 1.5$; (*b*) $t = 15$.

To sum up, the process of the interaction between the two drops can be described as follows:

(*a*) when S is small, the interaction is stronger, the trailing drop becomes much slower, and the leading drop becomes faster, which leads to a bigger S;

(*b*) when S is large, the interaction is weaker, the trailing drop becomes faster, and the leading drop becomes slower, which leads a smaller S.

Eventually, the equilibrium is reached, and both drops move with the same velocity with a fixed S.

4. The influence of S_0

The non-dimensional parameters in this section are the same as those in § 3, but with three values of S_0: 2.0, 2.5 (the benchmark run), and 3.0.

The discussion of the last paragraph in § 3 implies that the variance of S_0 does not influence S_F (figure 8). Also, the values of V_F for the three simulations are almost identical, which is clearly illustrated in figure 9. On the other hand, the variance of S_0 has a direct impact on the migration process (figure 9). It is easy to understand that, when S_0 is fairly large, the migration process of two drops is close to that of the corresponding isolated ones since the interaction between the drops is small. Figures 10 and 4 also reveal that the temperature difference between the front and rear stagnation points of the trailing drop is bigger for larger S_0: at $t = 15$, $(T(0) - T(\pi) \approx 1.0$ for $S_0 = 3.0$ while it is ≈ 0.9 for $S_0 = 2.0$; see dashed lines on the left-hand plots). That is, larger S_0 values lead to faster migration velocities at the early stages of simulations, which correspond to the faster decrease in drop distances for larger S_0 in figure 8. The trend of temperature difference of the leading drop is opposite (dashed lines on the right-hand plots), so even if S_0 is fairly large, the two drops are able to reach their common velocity. Moreover, for the temperature difference on the trailing drop, the larger S_0 means a faster transition to its final states, but it means a

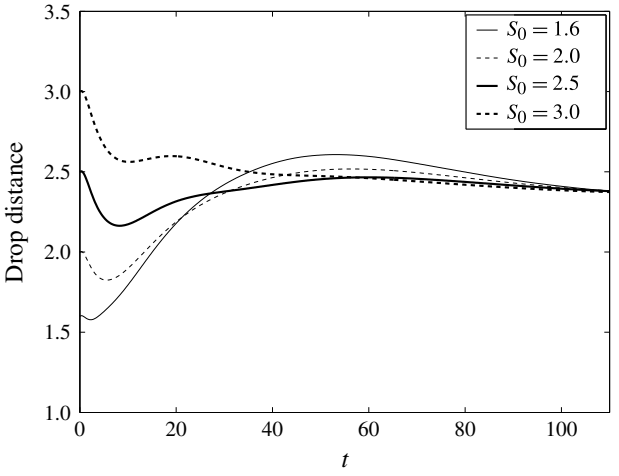

FIGURE 8. Time evolution of drop distances with different S_0. $Re = 1.2$, $\alpha = 0.14$, $\lambda = 0.47$, $\xi = 1.89$, $\gamma = 0.69$, $Ca = 0.04$, $Ma = 100$ and $\Lambda = 0.5$.

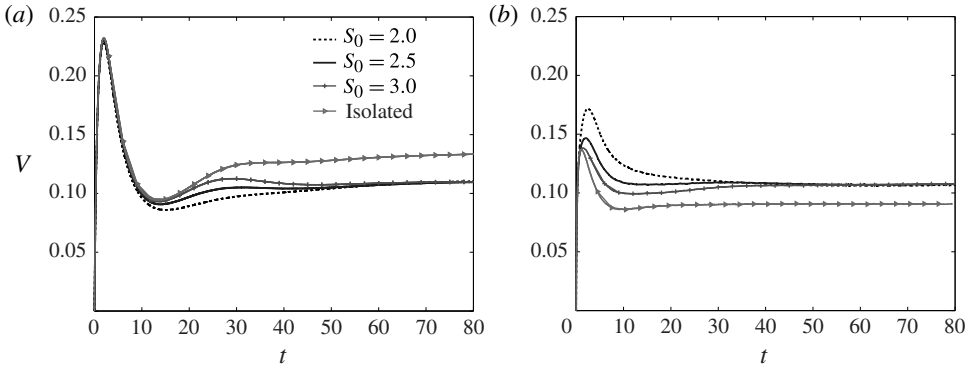

FIGURE 9. Time evolution of migrating drop velocities with different S_0. $Re = 1.2$, $\alpha = 0.14$, $\lambda = 0.47$, $\xi = 1.89$, $\gamma = 0.69$, $Ca = 0.04$, $Ma = 100$ and $\Lambda = 0.5$. (*a*) Trailing drop: $R = 1.0$; (*b*) leading drop: $R = 0.5$.

slower transition for the temperature difference on the leading drop (see figure 9 and the $t = 120$ curves in figures 10 and 4).

Note that the above discussion is true only when the values of S_0 are large enough. If S_0 is very small, the trailing drop might collide with the leading drop. (In our front-tracking solver, the interpolating function for the interface tension covers two grids (see more details in Tryggvason *et al.* 2001), and the region between two drops covers four grids in total. Thus, in this numerical work, the smallest possible S_0 is four times the grid size (or $0.04R$ if the computation grid is 400×2000 on the $4R \times 20R$ domain).)

5. The influence of Λ (radius ratio between the droplets)

The non-dimensional parameters in this section are the same as those in § 3, but with $\Lambda = 0.3$, 0.4 and 0.5.

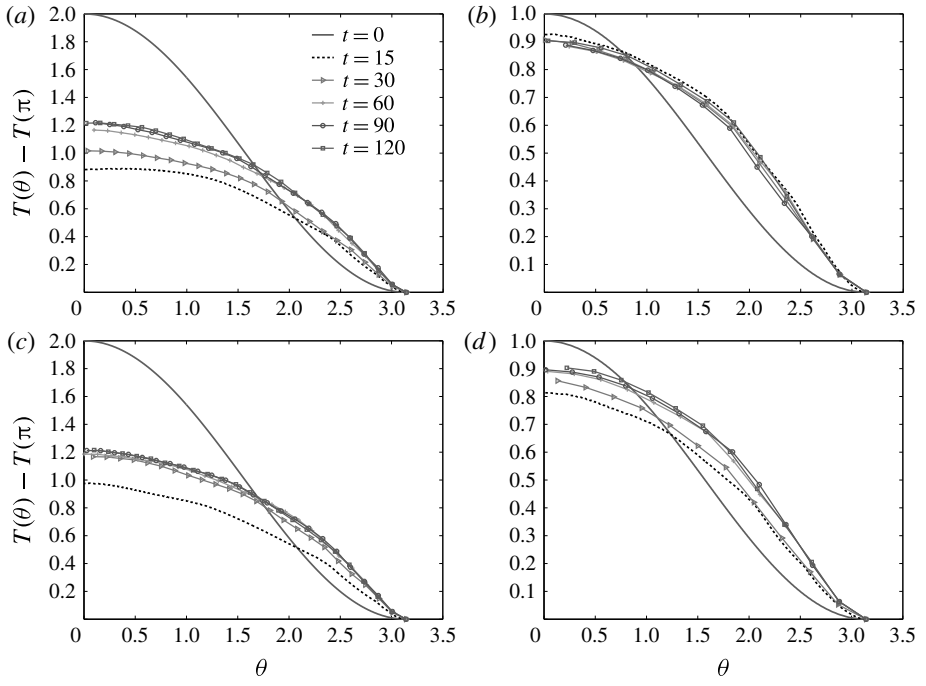

FIGURE 10. Scaled temperature distributions along the drop interfaces for different times with different S_0. $Re = 1.2$, $\alpha = 0.14$, $\lambda = 0.47$, $\xi = 1.89$, $\gamma = 0.69$, $Ca = 0.04$, $Ma = 100$ and $\Lambda = 0.5$. (*a*) Trailing drop: $R = 1.0$, $S_0 = 2.0$; (*b*) leading drop: $R = 0.5$, $S_0 = 2.0$; (*c*) trailing drop: $R = 1.0$, $S_0 = 3.0$; (*d*) leading drop: $R = 0.5$, $S_0 = 3.0$.

As can be seen from figure 11(*a*), there is almost no difference in the early processes of the trailing drop for different Λs. Figure 11 also shows that the final common migration velocity decreases for larger Λ. In a sense, this is counter to our general knowledge, because larger Λ means a larger leading drop, which should lead to larger V_F according to the results of isolated drops. A careful study of the final temperature fields shows that S_F is shorter for smaller Λ (figure 12), which means that the isotherms between the droplets are denser. This results in a larger temperature gradient along the drop interfaces, which finally leads to a larger migration speed.

The most interesting phenomenon for the leading drops is that the relative temperature differences between their initial states and their final ones become bigger for smaller Λ (figures 13*b* and 4*b*). In the case of $\Lambda = 0.3$, the difference after $t = 15$ is approximately 30 % larger than that at $t = 0$. For smaller Λ, a larger part of the leading drop is covered by the disturbed region in front of the front stagnation point of the trailing drop. As discussed in § 3, the isotherms accumulate in front of the trailing drop; hence, the relative temperature difference of the leading drop becomes larger. Therefore, although the absolute temperature difference on the leading drop still increases for larger Λ ($T(\pi) - T(0)$ is approximately 0.8 for $\Lambda = 0.3$, but approximately 0.9 for $\Lambda = 0.5$), the overall temperature gradient is $0.8/0.3 = 2.66$ for $\Lambda = 0.3$ at the final state, which is larger than that for $\Lambda = 0.5$ ($0.9/0.5 = 1.8$). This clearly explains why V_F is smaller for larger Λ.

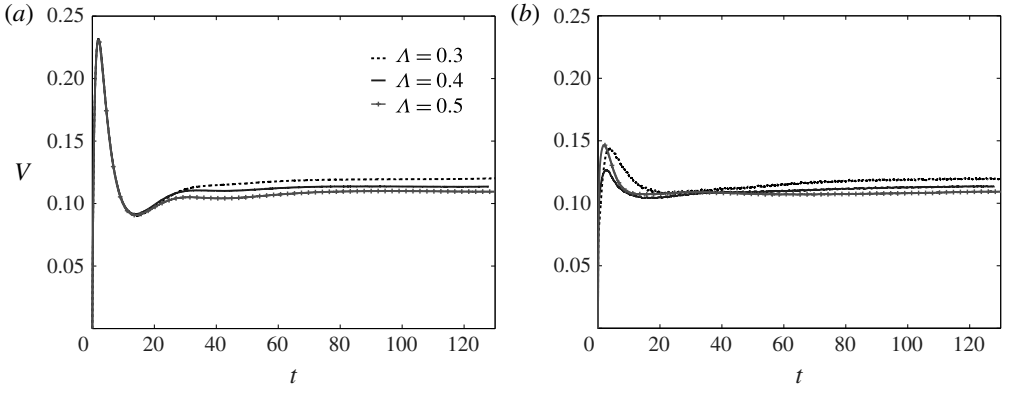

FIGURE 11. Time evolution of drop velocities for different Λ. $Re = 1.2$, $\alpha = 0.14$, $\lambda = 0.47$, $\xi = 1.89$, $\gamma = 0.69$, $Ca = 0.04$, $Ma = 100$ and $S_0 = 2.5$. (*a*) Trailing drop: $R = 1.0$; (*b*) leading drop: $R = \Lambda$.

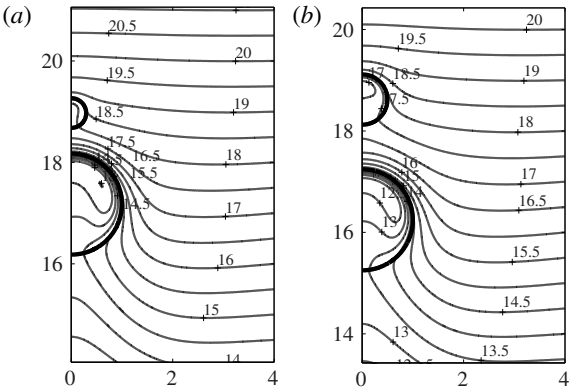

FIGURE 12. Temperature fields for different Λ at the final states ($t = 120$). $Re = 1.2$, $\alpha = 0.14$, $\lambda = 0.47$, $\xi = 1.89$, $\gamma = 0.69$, $Ca = 0.04$, $Ma = 100$ and $S_0 = 2.5$. (*a*) $\Lambda = 0.3$; (*b*) $\Lambda = 0.5$.

As already revealed in the benchmark run, the common V_F of both drops is bounded by the V_F values of the corresponding isolated ones. This conclusion can be made stronger, together with our earlier statement that 'smaller V_F for larger Λ': the common V_F value of both drops with $\Lambda < 0.5$ is bounded by the V_F values of the isolated ones when $\Lambda = 0.5$. Hence, the final V_F difference caused by various Λs is small, which is approximately 5 % at maximum (figure 11).

To further explore the influence of Λ, we extend the study with $\Lambda = 0.1, 0.15, 0.2, \ldots, 0.8$. When $\Lambda \geqslant 0.3$, the same resolution and time step are adopted as defined in the last paragraph of § 2. For smaller Λ, larger resolutions are adopted to guarantee enough grid points inside the small leading drops: for $\Lambda = 0.1, 0.15, 0.2$ and 0.25, the resolutions are 1000×5000, 800×4000, 600×3000 and 500×2500, and the time steps are $0.0004, 0.000625, 0.001$ and 0.001, respectively. For $\Lambda < 0.1$, a much finer resolution is required and current computers do not have such a capability.

When Λ is larger, the velocity gap between two corresponding isolated drops is smaller. Therefore, a weaker interaction is needed to maintain a final common speed

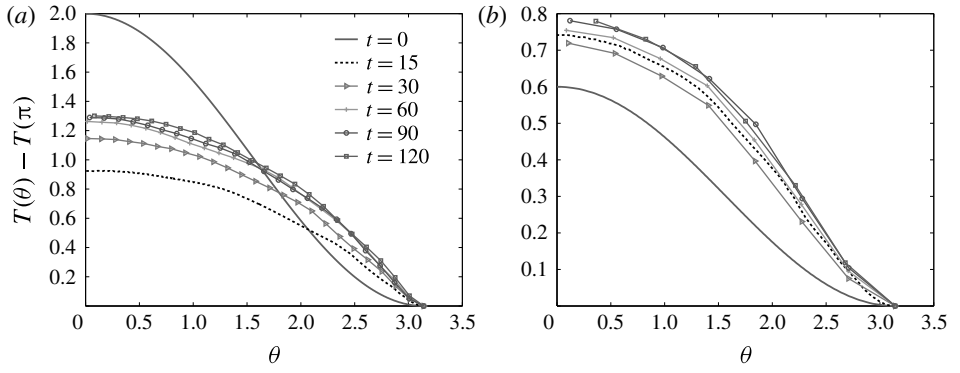

FIGURE 13. Scaled temperature distributions along the drop interfaces for different times with $\Lambda = 0.3$, $Re = 1.2$, $\alpha = 0.14$, $\lambda = 0.47$, $\xi = 1.89$, $\gamma = 0.69$, $Ca = 0.04$, $Ma = 100$ and $S_0 = 2.5$. (*a*) Trailing drop: $R = 1.0$; (*b*) leading drop: $R = 0.3$.

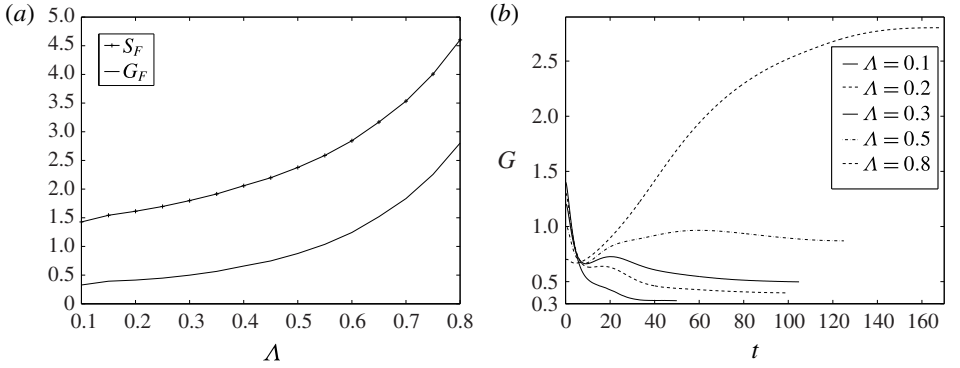

FIGURE 14. (*a*) Plot of final distance between drop centres and final gap between drop interfaces versus Λ, and (*b*) time evolution of gap between drops for different Λ. Note that, because the sizes of leading drops ($R\Lambda$) are not fixed in this section, it is more convenient to adopt G instead of S here. $Re = 1.2$, $\alpha = 0.14$, $\lambda = 0.47$, $\xi = 1.89$, $\gamma = 0.69$, $Ca = 0.04$, $Ma = 100$ and $S_0 = 2.5$.

of both drops, which readily leads to a larger S_F. This is more clearly shown in our simulations (figure 14*a*). When $\Lambda > 0.5$, the values of S_F increase exponentially.

When Λ is very small ($\Lambda = 0.1$), the big trailing drop dominates the interaction between drops, and the system reaches its final state quickly (figure 14*b*). When Λ is bigger, because the bigger leading drop causes a larger impact on the drop interaction, the interplay between two drops takes a longer time. Hence, a longer time and larger migration distance are needed to reach the final state for larger Λ. For $\Lambda > 0.8$, because of the migration distance limitation defined by (2.14), the two drops cannot reach a common migration speed.

Although G_F becomes smaller for smaller Λ, it does not drop down to zero as one might initially expect. The small-Λ lines in figure 14(*b*) show that the distance between the drops experience a more direct decrease at the beginning of the simulation, and becomes stable before the two drops collide. On the other hand,

Section	Ma	Re	α	λ	γ	ξ
6.1	10, 25, 50, 75, 100, 125, 150	1	1	1	1	1
6.2	50	1, 5, 10, 15, 20, 25, 30	1	1	1	1
6.3	100	1	2/5, 1/2, 2/3, 1, 3/2, 2, 5/2	1	1	1
6.4	100	1	1	2/5, 1/2, 2/3, 1, 3/2, 2, 5/2	1	1
6.5	100	1	1	1	2/5, 1/2, 2/3, 1, 3/2, 2, 5/2	1
6.6	100	1	1	1	1	2/5, 1/2, 2/3, 1, 3/2, 2, 5/2

TABLE 1. The non-dimensional numbers for all simulations in § 6. $S_0 \equiv 2.5$ and $\Lambda \equiv 0.5$.

the trend of the G_F line in figure 14(*a*) seems to show that the minimum value of G_F is around 0.3 even for the smallest Λ. Apparently, when Λ is small and Ma is fairly large, the accumulated isotherms around the head of the trailing drop become dominant in the system and effectively drive the small leading drop faster, and thus the drop collision is avoided.

6. The influence of non-dimensional numbers on non-deformable drops

In experiments in space, different Ma and Re can be set by changing the drop sizes and temperature gradients, whereas most other non-dimensional numbers are determined after experimental materials are chosen. To provide better support for future experiments, we will not focus on the parameters in space experiments in this section, but study the influence of each non-dimensional number with the others unchanged. Throughout this section, $S_0 \equiv 2.5$ and $\Lambda \equiv 0.5$. Ca is set to 0.04, hence the drops can be assumed to be non-deformable. Other parameters adopted in §§ 6.1–6.6 are specified in table 1.

Note that this study is dealing with drops (not bubbles), so their densities, viscosities, thermal conductivities, and specific heats are not very different from those of their mother liquids. Thus, the parameters in table 1 should be roughly sufficient to cover most situations in reality.

6.1. *The influence of Ma*

Not all time steps in this subsection are the same: 0.00025 for $Ma = 10$, 0.0005 for $Ma = 25$, 0.001 for $Ma = 50$ and 75, and 0.0015 for $Ma > 75$.

In a sense, the time evolution of migration velocities for double drops is just like the isolated ones (Yin *et al.* 2008): the variance of Ma leads to a similar initial accelerating process, but a larger Ma causes a bigger speed overshoot at the early

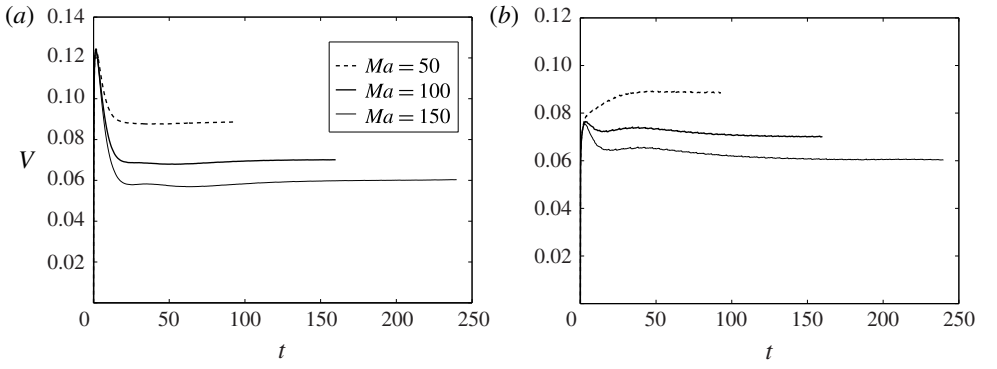

FIGURE 15. Time evolution of drop velocities for different Ma with $Ca = 0.04$ and $Re = \alpha = \lambda = \gamma = \xi = 1$. ($a$) Trailing drop: $R = 1.0$; (b) leading drop: $R = 0.5$.

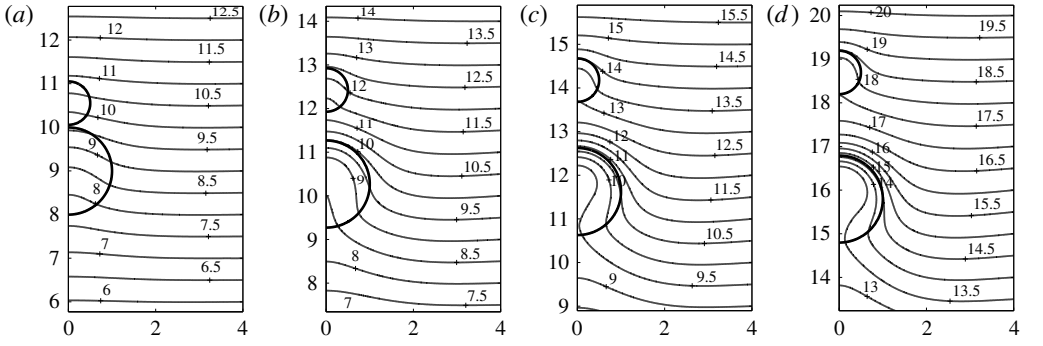

FIGURE 16. Temperature fields at final states for different Ma: (a) $Ma = 10$ ($t = 50$); (b) $Ma = 50$ ($t = 80$); (c) $Ma = 100$ ($t = 120$); (d) $Ma = 150$ ($t = 210$). $Ca = 0.04$ and $Re = \alpha = \lambda = \gamma = \xi = 1$.

time of the simulation, longer and more complicated process to reach the V_F, and lower V_F. Of course, due to the interaction process discussed earlier in this paper, the V_F of the double drops is lower than that of the isolated trailing drop (see figure 15).

It should be noted that the reference length is the radius of the trailing drop, and that the actual Ma of the leading drop is much smaller, so the velocity overshoots of the leading drops are never large (figure 15*b*). Figure 16(*a*) shows that the temperature distribution inside the leading drop for small Ma is quite close to that of the surrounding liquid at the same height, which means that the driving force determined by the temperature gradient experiences no dramatic decrease. This is unlike the cases with larger Ma (figure 16*b–d*). Therefore, there is no velocity 'overshoot' at all for the leading drop with a small Ma.

Compared with the corresponding plots with parameters from space experiments (figures 4, 10 and 13), the $t \neq 0$ temperature distributions along the trailing drop tend to gather in a relatively small region in this section, and they will not be discussed further in the following.

Earlier studies show that, for an isolated drop, a larger Ma leads to longer heat wake behind the drop (e.g. see figure 7 of Yin *et al.* 2012). To get a strong enough

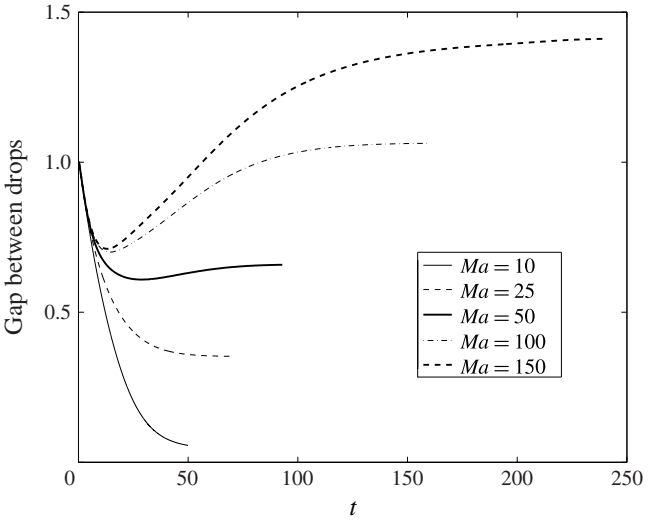

FIGURE 17. Time evolution of G for different Ma with $Ca = 0.04$ and $Re = \alpha = \lambda = \gamma = \xi = 1$.

interaction in the two-drop system, S_F needs to be smaller for a smaller Ma. Figure 17 shows that all simulations reach stable gaps eventually: G_F is approximately 1.4 for $Ma = 150$, while as low as 0.045 for $Ma = 10$. When Ma is even smaller, the heat wake behind the leading drop is even weaker, and so is the isotherm-gathering effect just above the trailing drop. Thus, the interaction mechanism between the drops is even weaker, and our numerical study shows that G_F will be so small that there is a good chance that the trailing drop may catch up with the leading drop when $Ma < 10$.

Most other simulations in this paper have Ma high enough ($\geqslant 50$) that G_F is always positive. Further comparison and discussion for creeping flows ($Ma < 10$) will be continued in § 9.3.

6.2. *The influence of Re*

Figure 18(*a*) shows that, for the trailing drops, small Re leads to bigger initial accelerating rates, sharper speed 'overshoots', and shorter periods to reach their V_F. These phenomena fit well with the conclusion drawn from the migration process of isolated drops (Yin *et al.* 2008). Without speed 'overshoots' for leading drops, figure 18(*b*) only shows that it takes a longer time with larger Re for the final states to be reached. Due to the interaction between drops, V_F mildly increases with increasing Re, and the corresponding isolated trailing drops show a much more obvious increase.

Despite the different Re, the temperature fields at the final states look identical (figure 19), the S_F are close to each other, and $T(0) - T(\pi) \approx 1.6$ for all trailing drops and ≈ 1.2 for all leading drops. The variance of Re does not change the final temperature differences along the interfaces of drops, but a bigger Re means that the temperature curve converges more slowly to the final state.

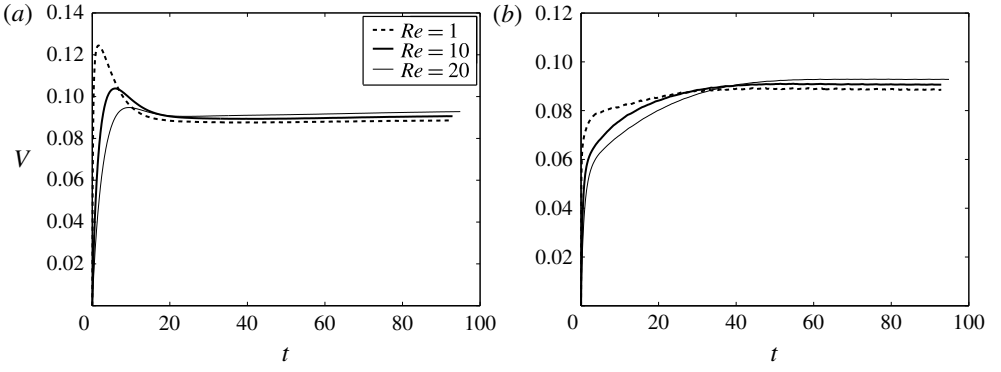

FIGURE 18. Time evolution of drop velocities for different Re with $Ma = 50$, $Ca = 0.04$ and $\alpha = \lambda = \gamma = \xi = 1$. (*a*) Trailing drop: $R = 1.0$; (*b*) leading drop: $R = 0.5$.

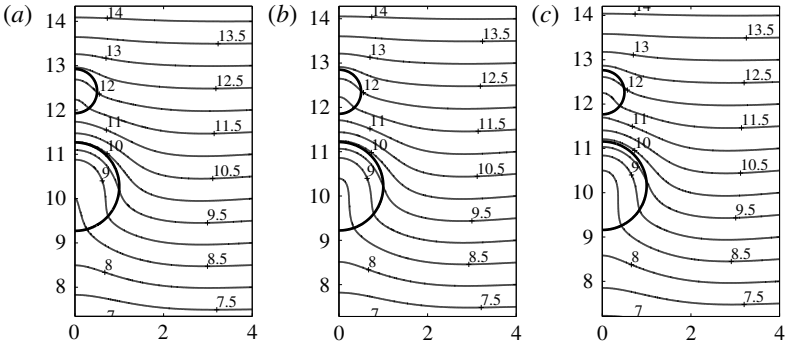

FIGURE 19. Temperature fields at the final state ($t = 80$) for different Re with $Ma = 50$, $Ca = 0.04$ and $\alpha = \lambda = \gamma = \xi = 1$. (*a*) $Re = 1$; (*b*) $Re = 10$; (*c*) $Re = 20$.

6.3. *The influence of α (viscosity ratio between the mother liquid and the drop)*

According to previous results (Yin *et al.* 2008), α is the most important parameter for isolated drops because its variance leads to a dramatic difference of drop velocities. For the two-drop system, the time evolutions for different α are also obviously distinguished from each other, and there is no overlap for any curves in both figures 20(*a*) and 20(*b*).

There are two mechanisms that influence the V_F of drops for different α:

(*a*) smaller α leads to better isothermal wrapping around the drops (figure 21), smaller temperature difference along the drop interface, and weaker driving force on the drops;

(*b*) smaller α also means smaller drop viscosities, or faster flow motion inside the drop, and the continuity of the flow speed near the interface makes the drop move faster.

In the case of isolated drops, the first mechanism is much weaker than the second one, so V_F increases super-linearly with the decrease of α. The existence of the

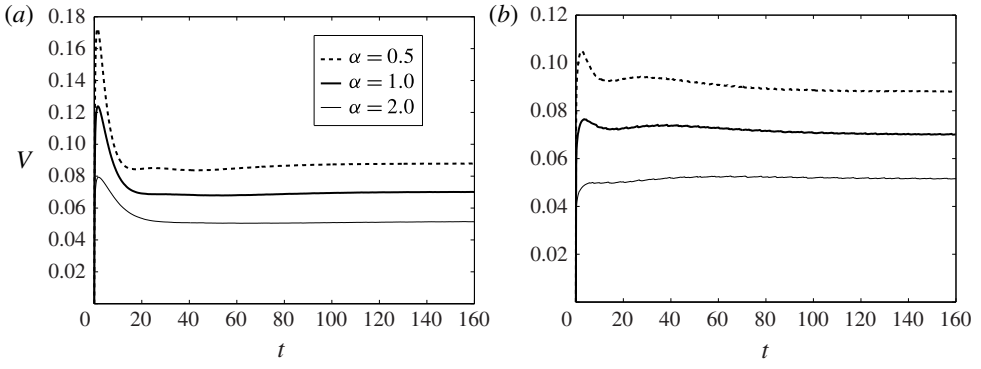

FIGURE 20. Time evolution of drop velocities for different α with $Ma = 100$, $Ca = 0.04$ and $Re = \lambda = \gamma = \xi = 1$. (*a*) Trailing drop: $R = 1.0$; (*b*) leading drop: $R = 0.5$.

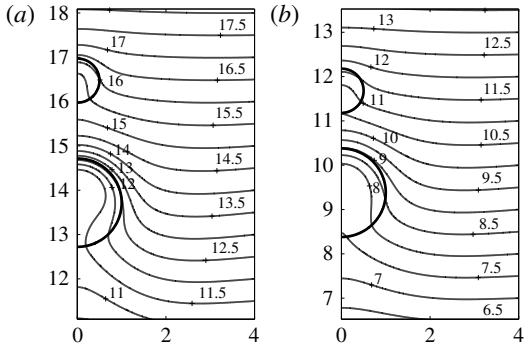

FIGURE 21. Temperature fields at the final states ($t = 120$) for different α with $Ma = 100$, $Ca = 0.04$ and $Re = \lambda = \gamma = \xi = 1$. (*a*) $\alpha = 0.5$; (*b*) $\alpha = 2.0$.

leading drop makes the first mechanism stronger for the trailing drop. Hence, V_F for the two-drop system does not experience very dramatic variance for different α.

The slower flow motion inside the leading drop for larger α results in the temperature at the bottom of the leading drop being closer to that of surrounding liquid at the same height, or results in a weaker heat wake. Hence, larger α means smaller S_F (figure 21), and this readily leads to a larger overall temperature difference for the leading drop. When $\alpha = 2.0$, the final temperature difference on the leading drop is higher than the initial difference.

6.4. *The influence of λ (thermal conductivity ratio between the mother liquid and the drop)*

Figure 22 clearly shows that a smaller λ causes stronger heat convection inside the drop, more isotherms accumulating around the front stagnant point, smaller temperature difference along the drop interface, and slightly smaller V_F. In comparison, the V_F of isolated drops shows a similar trend but more obvious difference for various β ($\beta := (\lambda/\xi\gamma)$, and $\beta = \lambda$ in this subsection because $\gamma = \xi = 1$ (Yin *et al.* 2008)).

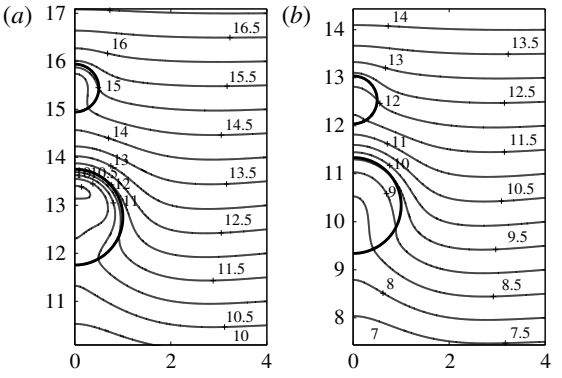

FIGURE 22. Temperature fields at the final states for different λ with $Ma = 100$, $Ca = 0.04$ and $Re = \alpha = \gamma = \xi = 1$. (*a*) $\lambda = 0.5$ ($t = 140$); (*b*) $\lambda = 2.0$ ($t = 100$).

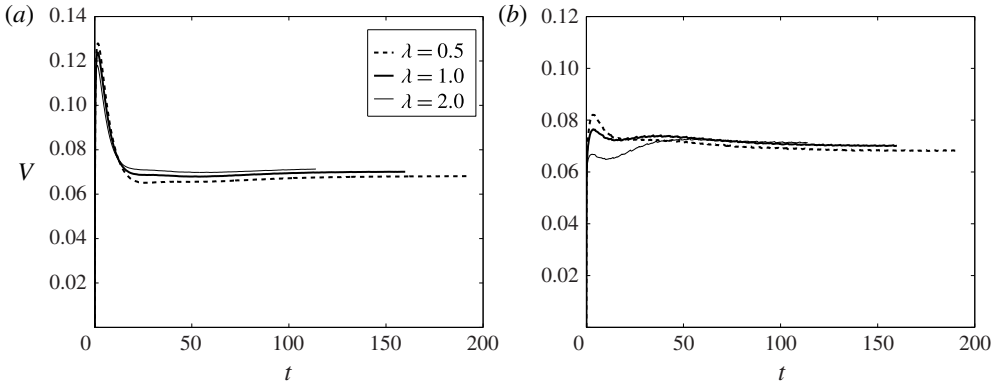

FIGURE 23. Time evolution of drop velocities for different λ with $Ma = 100$, $Ca = 0.04$ and $Re = \alpha = \gamma = \xi = 1$. (*a*) Trailing drop: $R = 1.0$; (*b*) leading drop: $R = 0.5$.

In general, the time evolution of velocities of trailing drops shows almost no difference for different λ, and those of leading drops differ more greatly from each other (figure 23). For all leading drops in this subsection, there are small overshoots in velocities. The leading drop velocity for $\lambda = 0.5$ becomes steady after the overshoot around $t = 20$, and that for $\lambda = 2.0$ has a quite long acceleration process after the overshoot and does not become steady until $t \approx 40$.

According to the definition of λ, larger λ means larger thermal diffusivity inside the drop, which results in the temperature at the bottom of the leading drop being closer to that of the surrounding liquid with the same height, or results in a weaker heat wake. Hence, larger λ means smaller S_F (figure 22).

On the other hand, larger thermal diffusivity causes fewer isotherms to accumulate around the front stagnant point of the trailing drop for larger λ. This accumulation decreases the temperature difference along the leading drop, and weakens the effect caused by smaller S_F. As a result, almost equivalent V_F values for different λ are obtained.

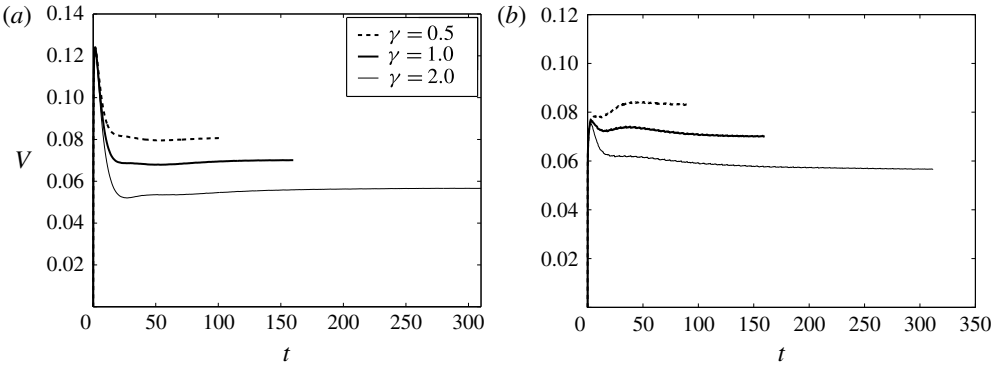

FIGURE 24. Time evolution of drop velocities for different γ with $Ma = 100$, $Ca = 0.04$ and $Re = \alpha = \lambda = \xi = 1$. (*a*) Trailing drop: $R = 1.0$; (*b*) leading drop: $R = 0.5$.

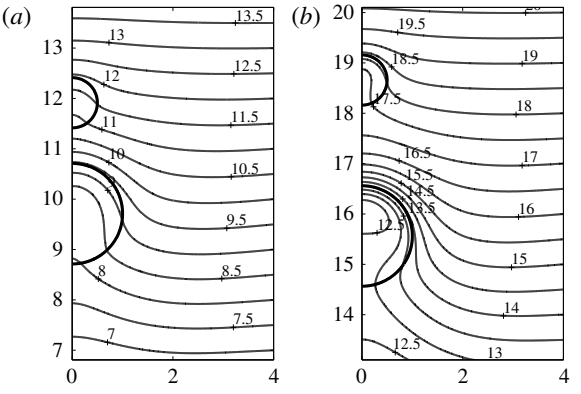

FIGURE 25. Temperature fields at the final states for different γ with $Ma = 100$, $Ca = 0.04$ and $Re = \alpha = \lambda = \xi = 1$. (*a*) $\gamma = 0.5$ ($t = 80$); (*b*) $\gamma = 2.0$ ($t = 220$).

6.5. *The influence of γ (specific heat ratio between the mother liquid and the drop)*

For the trailing drops, there is almost no difference in the early velocities for different γ (figure 24*a*). After the initial acceleration process, the speed of the $\gamma = 0.5$ drop quickly decreases to V_F, while that of the $\gamma = 2.0$ drop takes a longer time.

From the definition of γ, we know that larger γ means that the temperature fields inside the drops are less influenced by the background liquid, which means a smaller temperature difference along the drop interface (figure 25). For the leading drop, the temperature difference along the drop interface for $\gamma = 0.5$ keeps increasing until it reaches the steady state, while that for $\gamma = 2.0$ is always lower than the initial temperature difference. Hence, larger γ leads to lower V_F.

Previous studies on isolated drops clearly show that smaller γ leads to an obviously shorter heat wake behind the drop at the final states (e.g. see figure 28 in Yin *et al.* 2008). The large variance in the heat wake indicates that γ is an important factor that affects the interaction between two drops. For smaller γ, the shorter heat wake results in a smaller S_F, and the isotherms gathering around the front stagnant point of the trailing drop are closer to the leading drop, which further increases the overall temperature difference along the leading drop interface. The interaction makes the

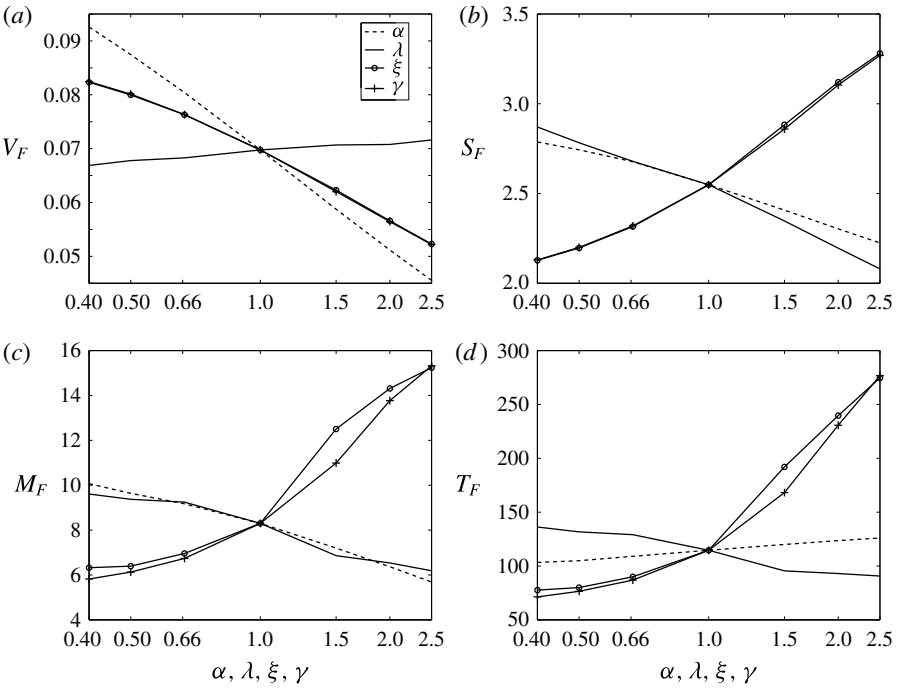

FIGURE 26. (*a*) Common velocity, (*b*) final distance between drops, (*c*) migration distance of the leading drop and (*d*) stable time, for various non-dimensional numbers ($\alpha, \lambda, \xi, \gamma$) with $Ma = 100$ and $Re = 1$. Note that the x-axes have logarithmic coordinates here.

drop with a smaller γ move even faster, or the variance of γ leads to a bigger V_F difference of pairs of drops than that of isolated drops.

6.6. *The influence of ξ (density ratio between the mother liquid and the drop)*

The variance of ξ has a similar effect on the drop interactions to that of γ, though the physical mechanism here is totally different. Larger ξ means that the drops are heavier, thus resulting in lower V_F. The faster motion of the drop with a smaller ξ leaves a shorter heat wake, and thus a smaller S_F. Also, the isotherms gathering around the front stagnant point of the trailing drop are closer to the leading drop for a smaller ξ, which further increases the temperature difference along the leading drop interface. In general, the drop interaction makes the drop with a smaller ξ move even faster, or the variance of ξ leads to a bigger V_F difference of pairs of drops than that of isolated drops.

6.7. *Final states*

The variance of V_F for various non-dimensional numbers is summarized in figures 26(*a*), 27(*a*) and 28(*a*). It is clear that V_F decreases with larger Re and λ, or with smaller α, ξ, γ, and Ma. On the other hand, the value of S_F seems to decrease with larger α, Re and λ, or with smaller ξ, γ and Ma (figures 26*b*, 27*a* and 28*a*). Although the variance of λ has almost no influence on the value of V_F, it has an obvious impact on S_F. Note that the variances of ξ and γ have almost the same effects on V_F and S_F.

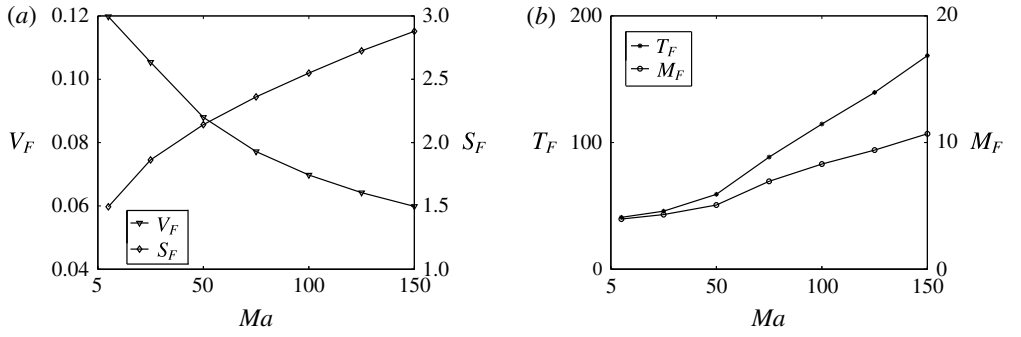

FIGURE 27. (*a*) Common velocity and final distance between drops, (*b*) migration distance of the leading drop and stable time, for various Ma with $Re, \alpha, \lambda, \xi, \gamma = 1$.

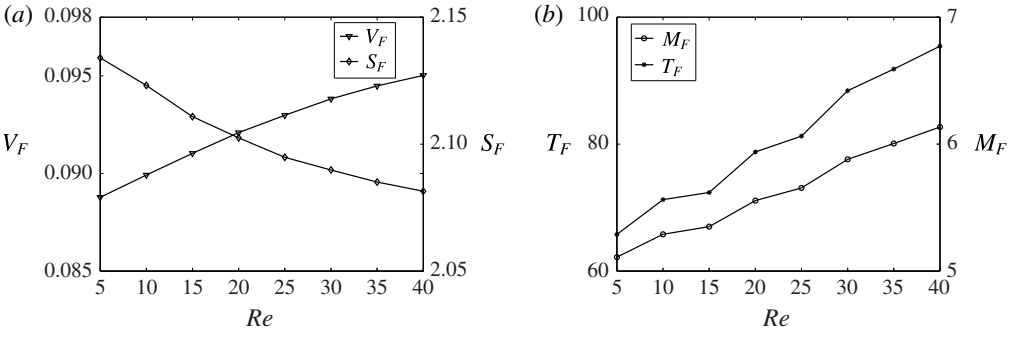

FIGURE 28. (*a*) Common velocity and final distance between drops, (*b*) migration distance of the leading drop and stable time, for various Re with $\alpha, \lambda, \xi, \gamma = 1$ and $Ma = 50$.

For reference in future space experiments, it is useful to discuss the migration distance required for the two-drop system to reach its final states. The biggest limitation in previous space experiments is that the tank was not long enough (Hadland *et al.* 1999), so we only study the migration distance of the leading drop (M_F). Figures 26(*c*), 27(*b*) and 28(*b*) show that larger Ma, Re, ξ and γ, or smaller α and λ, lead to longer migration distances.

Most variances of T_F with non-dimensional numbers show similar trends to those of M_F (figures 26*d*, 27*b* and 28*b*). One exception is the influence of α. Although T_F slightly increases for larger α, M_F obviously decreases because of the dramatically decreasing V_F for larger α.

7. The interaction of deformed drops

For creeping flow, Haj-Hariri *et al.* (1990) showed that, depending on whether the drop density is larger or smaller than that of the exterior fluid, the deformed drop shape will be a prolate (for $\xi > 1$) or an oblate spheroid (for $\xi < 1$), respectively. For fairly large Ma and Re values, Chang *et al.* (2011) observed similar phenomena with a numerical simulation.

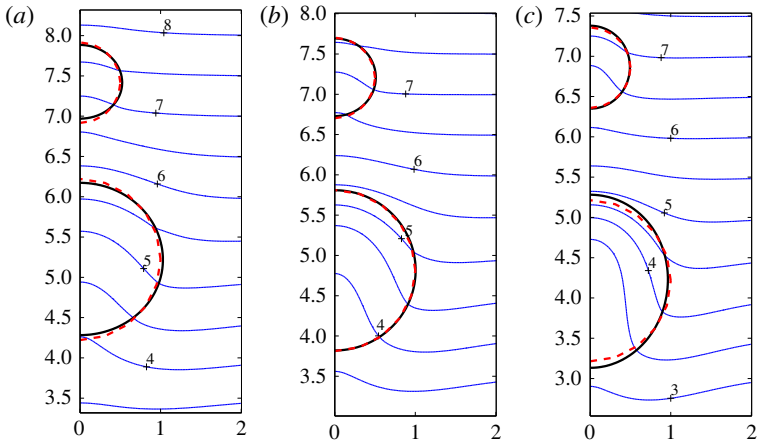

FIGURE 29. (Colour online) Temperature fields at $t = 20.0$ for different ξ with $Ca = 0.2$, $Re = 50.0$, $Ma = 50.0$, $\alpha = \gamma = 0.5$, $\lambda = 0.25$. The solid black circles indicate the locations of interfaces, and the dashed grey circles (red online) indicate the interfaces if there is no drop deformation at all. (*a*) $\xi = 0.5$; (*b*) $\xi = 1.0$; (*c*) $\xi = 2.0$.

To make this paper concise, except for Ca and ξ, we do not vary other parameters as we did in § 6. In this section, Ca is set to be fairly large to achieve clear drop deformation, and three values are chosen: 0.1, 0.15 and 0.2. Also, $\xi = 0.25$, 0.5, 1, 2.0 and 4.0 are chosen. For the rest of the parameters, $\Lambda = 0.5$, $S_0 = 2.5$, $Re = 50.0$, $Ma = 50.0$, $\alpha = \gamma = 0.5$ and $\lambda = 0.25$. Note that Re in this section is also fairly large to achieve clear deformation. In this section, the resolution is 300×1500, and the time step is 0.0001.

Note that Ca was set to 0.04 in simulations in other sections, which means that the migration limitation defined by (2.14) need not be a concern since M_F in those simulations is always below 20.0. However, to avoid negative interfacial tensions, the simulations in this section are stopped much earlier than those non-deformable cases. For example, because $M_l = 2.0$ for $Ca = 0.2$, all simulation must be stopped before $T_S = 20$.

To keep this paper concise, only figures for $Ca = 0.2$ runs are presented. Figure 29 clearly shows that there is no obvious drop deformation for $\xi = 1.0$, the $\xi = 0.5$ drops become flattened while the $\xi = 2.0$ drops are elongated in the z direction. This is in good agreement with the corresponding findings for single deformed drops (see figure 13 in Chang *et al.* 2011).

The heat wakes behind the leading drops are quite different from those of non-deformable drops. For large-Ca runs, the elongated leading drop with $\xi = 2.0$ has a much weaker heat wake than the flattened leading drop with $\xi = 0.5$; the non-deformable drops show the opposite trend (see the discussion in § 6.6). It is clear that the short migration distance is not enough for the two drops to reach their common velocity (figure 30), so there is no discussion on final states in this section.

When Ca is smaller, the drop deformation is also smaller in the same migration period. In the case of $Ca = 0.1$, there is almost no deformation for all ξ values at $t = 20$. On the other hand, because small Ca means larger M_l, the small-Ca runs can be continued much longer before they are stopped (for $Ca = 0.1$, $T_S = 54$ for $\xi = 0.25$ and $T_S = 82$ for $\xi = 4.0$). Eventually, the drop deformations are also quite large.

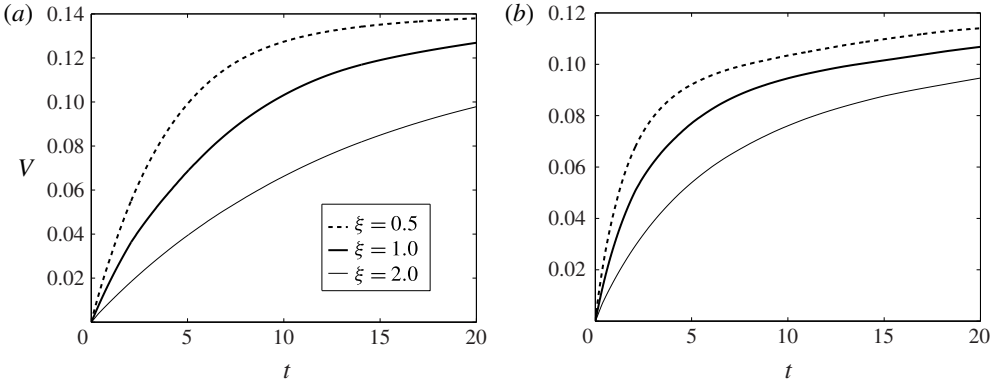

FIGURE 30. Time evolution of drop velocity for different ξ with $Ca = 0.2$, $Re = 50.0$, $Ma = 50.0$, $\alpha = \gamma = 0.5$, $\lambda = 0.25$. (*a*) Trailing drops; (*b*) leading drops.

When Ca is even smaller (e.g. $Ca = 0.04$, as for the rest of the simulations in this paper), it takes a longer time for drop deformations to become noticeable, and the two drops may have a better chance of reaching a common velocity.

8. The comparison between numerical solutions and experimental results

In Balasubramanian *et al.* (1996) and later in § 7.11.3 of Subramanian & Balasubramaniam (2001), some space experiments on drop interactions were described with Fluorinert FC-75 drops and the continuous phase of DC-200 silicone oil of nominal viscosity 50 cSt. The Marangoni number for their trailing drop is 102, and Λ = (2.40 mm/4.72 mm) = 0.508, both of which are close to those adopted in § 3. The effect of the leading drop heat wake on the trailing drop was analysed by Balasubramanian & Subramanian (1999), assuming Ma and $Re \to \infty$.

It should be noted that there are quite different initial conditions between numerical simulations and experiments.

(*a*) In our numerical simulation, both drops start to migrate simultaneously. There is only a very weak interaction between drops initially, hence the trailing drop accelerates at a rate close to that of an isolated one. Before the heat wake behind the leading drop takes effect, the trailing drop has already achieved a relatively high migration velocity.

(*b*) In space experiments, the leading drop is first injected into the tank, and it starts to migrate immediately, leaving the heat wake behind. The trailing drop is injected when the original constant temperature gradient is changed by the heat wake of the leading drop, and it has a much slower acceleration than if isolated. In fact, the heat wake may also lead to a more difficult injection process for the trailing drop since the thermocapillary driving force is also weaker. This might be one of the reasons why the interaction experiments are 'relatively difficult' to perform (Balasubramanian *et al.* 1996).

To have a better understanding of why there are only a few successful space experiments on this subject, we adopted the parameters of the 'successful' one (Balasubramanian *et al.* 1996): $Ma = 102.0$, $Re = 0.26$, $\xi = 1.89$, $\alpha = 0.028$, $\lambda = 0.47$, $\gamma = 0.69$, $\Lambda = 0.508$, $Ca = 0.04$, and performed the following two simulations: Run 1 for two drops; and Run 2 for an isolated drop.

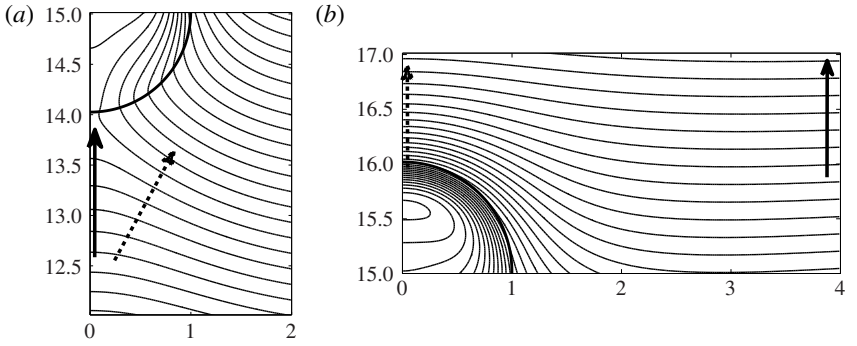

FIGURE 31. Run 2: temperature distributions around the drop at $t = 60$ with $Ma = 102.0$, $Re = 0.26$, $\xi = 1.89$, $\alpha = 0.028$, $\lambda = 0.47$, $\gamma = 0.69$, $\Lambda = 0.508$ and $Ca = 0.04$. Different parts of the same temperature field are shown here: *a*) behind the drop, *b*) above the drop. In each plot, the temperature gradient indicated by the dashed arrow is higher than that indicated by the solid arrow.

Figure 31 show the temperature distribution around the drop at the final state of Run 2. Figure 31(*a*) clearly shows that, for the region just behind the drop, the temperature gradient in the vertical direction (solid arrow) is lower than that slanting to its right (dashed arrow). In experiments, this means that if the two drops are close and in aligned arrangement the system is unstable because the trailing drop will move towards the direction with the highest temperature gradient. Hence, the big trailing drop most likely will override the small leading drop. And without the big drop trailing behind, the small drop may migrate more slowly at a speed close to that of its corresponding isolated drop. When the big drop becomes the leading drop, it will move even faster, and leave the small drop far behind. Each drop will migrate at the same speed as its corresponding isolated one, the distance between two drops becomes larger and larger, and there is almost no drop interaction then.

On the other hand, α is very small in these two simulations, which means that it takes a very long time for the drops to reach their V_F. Figure 32 shows that the time evolution of S in Run 1 is much more complicated than that of the benchmark run in § 3 (figure 2*b*), and that S keeps decreasing until a very late time. This means that the drop interaction is never strong, and the symmetry-breaking mechanism discussed in the previous paragraph never happens. So in space experiments, it has been observed that the leading drop moves virtually as if it were isolated. However, the trailing drop moves more slowly than if it were isolated. Apparently, the leading drop influences the trailing drop, but the trailing one does not affect the leading one.

For the successful implement of corresponding experiments, we provide two suggestions.

(*a*) Carefully design the experimental setup: the experimental materials, drop sizes, the temperature gradient, etc. With proper non-dimensional parameters, the strong drop interaction can be avoided.

(*b*) Introduce some other mechanism to keep the symmetry of the system. One possible way is choosing a slender tank. The temperature gradient on the boundary (solid arrow in figure 31*b*) is lower than that in the centre (dashed arrow in figure 31*b*), and drops near the wall tend to move away from the boundary. With a slender tank, drops will be confined in the central region of the tank, and the symmetry adopted in this paper will not be broken even if the drop interaction is strong.

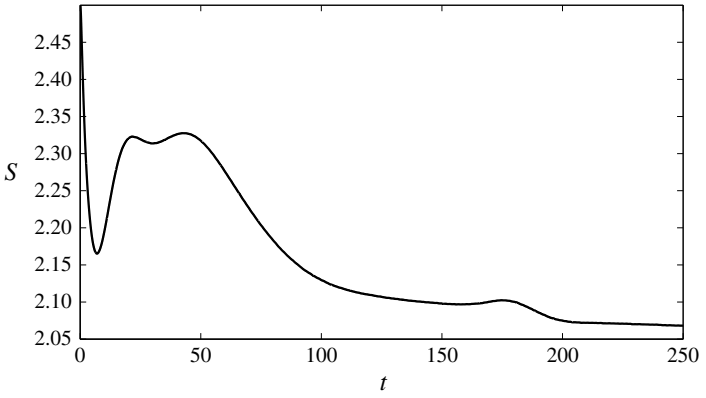

FIGURE 32. Run 1: time evolution of the drop distance with $Ma = 102.0$, $Re = 0.26$, $\xi = 1.89$, $\alpha = 0.028$, $\lambda = 0.47$, $\gamma = 0.69$, $\Lambda = 0.508$ and $Ca = 0.04$.

9. Comparisons between the current results and those of creeping flows

9.1. *Some comparisons on the interactions of bubbles*

Meyyappan, Wilcox & Subramanian (1983) investigated the axisymmetric thermocapillary migration of two bubbles in the quasi-static state by using the bispherical coordinate system (mathematical model similar to that used by Stimson & Jefferey 1926). As expected, they found that the interaction effect between two bubbles increases as the separation distance is decreased. A small bubble moves more rapidly in the presence of a larger bubble than in its absence, whether it leads or trails the larger bubble. However, they found that the velocity of the large bubble is reduced compared to the case when it is isolated, but to a *lesser* extent. Also, they illustrated that two equal-sized bubbles move with the same velocity as if they were isolated (when the bubbles are of equal diameter, they exert no influence on each other's velocity for all separation distances and such remarkable result is due to the exact cancellation of the thermal and fluid mechanical two-body interactions). Later, Feuillebois (1989) presented a theoretical confirmation of this numerical conclusion.

However, the above scheme cannot provide the details of the transient process as we do in this paper, so only the results of the final steady states are compared in the following. In our research, the small drop is always the leading one, and it always moves faster than the case when it is isolated, which is just the same as shown in the above paragraph. But because of the stronger heat wake in this study, our findings have two major differences from those of creeping flows:

(*a*) according to figure 2(*a*), the velocity difference between the big trailing drop and the corresponding isolated one is bigger than the difference with the small drop (see the italic text in the above paragraph);

(*b*) from figure 14(*a*), it can be concluded that S_F will be larger for larger Λ. It can be expected that, when S_F is quite large, drops may also move with the same velocity as if they were isolated, just like the case of bubbles. However, because of the limitation of M_l (2.14), the final states when $\Lambda > 0.8$ are never reached.

9.2. *Some comparisons on the interactions of non-deformable drops*

Spherical drops undergoing thermocapillary migration in a dilute dispersion were studied by Zhang & Davis (1992). With conducting drops considered, they found

that increases in the thermal conductivity and/or viscosity of the drop fluid decrease the collision efficiency due to the effects of hydrodynamic and thermocapillary interactions. In particular, the relative velocity of two unequal drops can change sign as they become very close to each other, if the thermal conductivity of the drop fluid is sufficiently large compared with that of the surrounding fluid (the relative drop velocity can reverse its sign when the two drops become close because the smaller drop experiences an increased temperature gradient resulting from the larger drop distorting the imposed temperature gradient; and as a result, the smaller drop moves away from the larger one). Under these conditions, drop collision does not occur unless there are other driving forces such as an attractive van der Waals force.

In comparison, the large-Ma simulations in this paper reveal more complicated processes. If we concentrate on figure 2(a), it can be seen that the relative velocity of the two drops changes sign twice: around $t = 8$ and $t = 60$. For the simulations in § 6, the situations are much more complicated:

(a) in § 6.1, there is no sign changing for $Ma < 25$, correspondingly there is no overshoot in drop velocities, and the heat wakes are very weak;

(b) in § 6.2, all $Re \geqslant 5$ runs change sign twice because higher Re can cause more fluctuations in flows;

(c) there is one sign change for each of the other simulations in § 6.

9.3. *Some comparisons on the interactions of deformable drops*

Before this work, the effect of deformability was studied mostly by a perturbation technique assuming small deformations; some recent analyses within the framework of boundary integral methods ($Re \to 0$) are due to Zhou & Davis (1996), Berejnov, Lavrenteva & Nir (2001) and Rother, Zinchenko & Davis (2002).

(a) The axisymmetric motion and deformation of two viscous drops in a temperature field with an imposed gradient along their line of centres were studied by Zhou & Davis (1996). The effects of the capillary number, the drop size ratio, and the drop-to-medium conductivity ratio on drop motion and deformation are illustrated. It is found that the hydrodynamic interactions between the drops has a stronger effect on the smaller of the two drops, in terms of both drop motion and drop deformation. Deformation has a large effect on the rate of drainage of the thin film between the drops, but relatively little effect on the velocities of the drop centres. The numerical results also verify that small drop deformations reduce the film drainage rate and prevent drop coalescence in the absence of attractive forces.

As a comparison, the main mechanism leading to deformation in their study is $G \to 0$, which only corresponds to the $Ma < 10$ simulations in § 6.1 of this paper. The drop coalescence has to be taken into consideration when $G \to 0$, which will be done in our future investigation. The above investigation may also neglect the limitation on M_l, and the interfacial tension may become negative in some simulations (see figure 2(e) in Zhou & Davis 1996).

(b) Berejnov *et al.* (2001) focused on equal-viscosity fluids and on cases when drops are of equal radii or when a smaller drop trails behind a larger drop. For equal-sized drops, they found that the motion of a leading drop is retarded while the motion of the trailing one is enhanced compared with the undeformable case, and that the distance between the centres of equal-sized deformable drops decreases with time. When a small drop follows a large one, two patterns of

behaviour may exist. For moderate or large initial separation the drops separate. However, if the initial separation is small there is a transient period in which the separation distance initially decreases and only afterward the drops separate. They considered the fact that the interfacial tension may become negative in their simulations. With $\xi = 1$, either near-zero G or near-zero interfacial tension is necessary to cause the drop deformation in their simulations (see figures 9(a) and 12 in Berejnov *et al.* 2001).

Rother *et al.* (2002) performed a full three-dimensional simulation on this issue. Relative trajectories for two deformable drops were calculated for different values of the drop size ratio, drop-to-medium thermal conductivity ratio, and viscosity ratio, and then compared with those for spherical and slightly deformable drops. Results indicate that deformation increases the minimum separation and inhibits coalescence.

We stop the code before M_l is reached, but Rother *et al.* (2002) avoid the limitation of migration distance by moving the reference point of interfacial tension along with the leading drop. It is clear that our treatment is closer to the physical reality than theirs. Also, the main reason for drop deformation in our simulations is $\xi \neq 1$, which has not been investigated in their studies. The negative or near-zero interfacial tension is avoided in our research.

10. Conclusions

In this paper, we study the thermocapillary migration of a smaller drop followed by a bigger one under the axisymmetric assumption. Various cases are considered by changing the relevant non-dimensional numbers. The order of magnitude of the studied Marangoni number is $O(100)$, and thus some phenomena related to real flows are revealed. When Marangoni numbers are relatively large, thin thermal boundary layers develop along the liquid–liquid interface, leading to the formation of thermal wakes at the rear of a moving drop. The thermal wake field of the leading drop wraps around the trailing drop, and has a significant impact on its motion.

Our study find that, unless two drops are very close initially, the variance of initial distance between the drop centres, S_0, does not influence the final state but leads to obviously different migration processes. When the leading drop is larger, the interaction process takes a much longer time for the two drops to reach their common velocities. For large Ma, no matter how small Λ is, the trailing drop cannot catch up with the leading one.

The influence of six non-dimensional numbers on drop interactions is also studied. It is found that V_F decreases with larger Re and λ, or with smaller α, ξ, γ, and Ma; the value of S_F decreases with larger α, Re and λ, or with smaller ξ, γ and Ma. The variance of λ has almost no influence on the value of V_F, but it has an obvious impact on S_F. The variances of ξ and γ have almost the same effects on V_F and S_F.

The interaction between deformed drops is also studied when $\xi \neq 1$ and the capillary number is fairly large. The elongated leading drop with $\xi > 1$ has a weaker heat wake than the flattened leading drop with $\xi < 1$, while non-deformable drops show the opposite trend.

Acknowledgements

This project is supported by NSF of China (Contracts No. G11472283 and G11172308). The authors wish to thank Professor Y. P. Zhang for many valuable discussions and for her critical reading of the manuscript. Z.Y. thanks Professor

J. C. Xie, Dr W. T. Bi, and Professor R. S. Subramanian for their helpful discussions on physical problems and Dr Q. Kang and Dr L. Duan for discussing some of their experimental details. Q.L. thanks Mr K. Y. Lou, Dr L. Chang and Dr K. Yang for their technical and scientific support. Professor W. R. Hu provides invaluable support for this work. The authors are indebted to the three anonymous referees for their extremely detailed advice and drawing the authors' attention to more previous works in this field.

REFERENCES

ANDERSON, J. 1985 Droplet interactions in thermocapillary motion. *Intl J. Multiphase Flow* **11**, 813–824.

BALASUBRAMANIAM, R. & CHAI, A. 1987 Thermocapillary migration of droplets – an exact solution for small Marangoni numbers. *J. Colloid Interface Sci.* **119**, 531–538.

BALASUBRAMANIAN, R., LACY, C., WONIAK, G. & SUBRAMANIAN, R. 1996 Thermocapillary migration of bubbles and drops at moderate values of the Marangoni number in reduced gravity. *Phys. Fluids* **8**, 872–880.

BALASUBRAMANIAN, R. & SUBRAMANIAN, R. 1999 Axisymmetric thermal wake interaction of two bubbles in a uniform temperature gradient at large Reynolds and Marangoni numbers. *Phys. Fluids* **11**, 2856–2864.

BEREJNOV, V., LAVRENTEVA, O. M. & NIR, A. 2001 Interaction of two deformable viscous drops under external temperature gradient. *J. Colloid Interface Sci.* **242**, 202–213.

BORCIA, R. & BESTEHORN, M. 2007 Phase-field simulations for drops and bubbles. *Phys. Rev.* E **75**, 056309.

BRADY, P., HERRMANN, M. & LOPEZ, J. 2011 Confined thermocapillary motion of a three-dimensional deformable drop. *Phys. Fluids* **23**, 022101.

CHANG, L., YIN, Z. & HU, W. 2011 Transient behavior of the thermocapillary migration of drops under the influence of deformation. *Sci. Sin.* **41**, 960–968.

CHEN, J. & LEE, T. 1992 Effect of surface deformation on thermocapillary bubble migration. *AIAA J.* **30**, 993–998.

CHOUDHURI, D. & RAJA SEKHAR, G. 2013 Thermocapillary drift on a spherical drop in a viscous fluid. *Phys. Fluids* **25**, 043104.

FEUILLEBOIS, F. 1989 Thermocapillary migration of two equal bubbles parallel to their line of centers. *J. Colloid Interface Sci.* **131**, 267–274.

FROLOVSKAYA, O., NIR, A. & LAVRENTEVA, O. M. 2006 Stationary regimes of axisymmetric thermal wake interaction of two buoyant drops at low Reynolds and high Peclet number. *Phys. Fluids* **18**, 072103.

HADLAND, P., BALASUBRAMANIAM, R., WOZNIAK, G. & SUBRAMANIAN, R. 1999 Thermocapillary migration of bubbles and drops at moderate to large Marangoni number and moderate Reynolds number in reduced gravity. *Exp. Fluids* **26**, 240–248.

HAJ-HARIRI, H., NADIM, A. & BORHAN, A. 1990 Effect of inertia on the thermocapillary velocity of a drop. *J. Colloid Interface Sci.* **140**, 277–286.

HAJ-HARIRI, H., SHI, Q. & BORHAN, A. 1997 Thermocapillary motion of deformable drops at finite Reynolds and Marangoni numbers. *Phys. Fluids* **9**, 845–855.

KEH, H. & CHEN, S. 1990 The axisymmetric thermocapillary motion of two fluid droplets. *Intl J. Multiphase Flow* **16**, 515–527.

KEH, H. & CHEN, S. 1992 Droplet interactions in axisymmetric thermocapillary motion. *J. Colloid Interface Sci.* **151**, 1–16.

LAPPA, M. 2005 Assessment of VOF strategies for the analysis of Marangoni migration, collisional coagulation of droplets and thermal wake effects in metal alloys under microgravity conditions. *Comput. Mater. Continua* **2**, 51–64.

LAVRENTEVA, O. M. & NIR, A. 2003 Axisymmetric thermal wake interaction of two drops in a gravity field at low Reynolds and high Peclet numbers. *Phys. Fluids* **15**, 3006–3014.

LEE, T. & KEH, H. 2013 Axisymmetric thermocapillary migration of a fluid sphere in a spherical cavity. *Intl J. Heat Mass Transfer* **62**, 772–781.

LESHANSKY, A. M. & NIR, A. 2001 Thermocapillary alignment of gas bubbles induced by convective transport. *J. Colloid Interface Sci.* **240**, 544–551.

LI, Q. 2013 Thermocapillary migration and interactions of two drops. Master's thesis, Institute of Mechanics, Chinese Academy of Sciences.

LIU, H., VALOCCHI, A., ZHANG, Y. & KANG, Q. 2013 Phase-field-based lattice Boltzmann finite-difference model for simulating thermocapillary flows. *Phys. Rev.* E **87**, 013010.

LIU, H., ZHANG, Y. & VALOCCHI, A. 2012 Modeling and simulation of thermocapillary flows using lattice Boltzmann method. *J. Comput. Phys.* **231**, 4433–4453.

LOEWENBERG, M. & DAVIS, R. H. 1993 Near-contact thermocapillary motion of two non-conducting drops. *J. Fluid Mech.* **256**, 107–131.

MEYYAPPAN, M., WILCOX, W. R. & SUBRAMANIAN, R. S. 1983 The slow axisymmetric motion of two bubbles in a thermal gradient. *J. Colloid Interface Sci.* **94**, 243–257.

NAS, S., MURADOGLU, M. & TRYGGVASON, G. 2006 Pattern formation of drops in thermocapillary migration. *Intl J. Heat Mass Transfer* **49**, 2265–2276.

NAS, S. & TRYGGVASON, G. 2003 Thermocapillary interaction of two bubbles or drops. *Intl J. Multiphase Flow* **29**, 1117–1135.

ROTHER, M. A., ZINCHENKO, A. Z. & DAVIS, R. H. 2002 A three-dimensional boundary-integral algorithm for thermocapillary motion of deformable drops. *J. Colloid Interface Sci.* **245**, 356–364.

SCHEDIN, S. 2006 Digital holographic interferometry. *J. Hologr. Speckle* **3**, 1–17.

STIMSON, M. & JEFFEREY, G. B. 1926 The motion of two spheres in a viscous fluid. *Proc. R. Soc. Lond.* A **111**, 110–116.

SUBRAMANIAN, R. & BALASUBRAMANIAM, R. 2001 *The Motion of Bubbles and Drops in Reduced Gravity*. Cambridge University Press.

SUBRAMANIAN, R., BALASUBRAMANIAM, R. & WOZNIAK, G. 2002 Fluid mechanics of bubbles and drops. In *Physics of Fluids in Microgravity* (ed. R. Monti), pp. 149–177. Taylor & Francis.

SUN, R. & HU, W. 2002 The thermocapillary migrations of two bubbles in microgravity environment. *J. Colloid Interface Sci.* **255**, 375–381.

SUN, R. & HU, W. 2003 Planar thermocapillary migration of two bubbles in microgravity environment. *Phys. Fluids* **15**, 3015–3027.

TREUNER, M., GALINDO, V., GERBETH, G., LANGBEIN, D. & RATH, H. J. 1996 Thermocapillary bubble migration at high Reynolds and Marangoni numbers under low gravity. *J. Colloid Interface Sci.* **179**, 114–127.

TRYGGVASON, G., BUNNER, B., ESMAEELI, A., JURIC, D., AL-RAWAHI, N., TAUBER, W., HAN, J., NAS, S. & JAN, Y.-J. 2001 A front-tracking method for the computations of multiphase flow. *J. Comput. Phys.* **169**, 708–759.

WELCH, S. 1998 Transient thermocapillary migration of deformable bubbles. *J. Colloid Interface Sci.* **208**, 500–508.

WOZNIAK, G., BALASUBRAMANIAM, R., HADLAND, P. & SUBRAMANIAN, R. S. 2001 Temperature fields in a liquid due to the thermocapillary motion of bubbles and drops. *Exp. Fluids* **31**, 84–89.

WU, Z. & HU, W. 2013 Effects of Marangoni numbers on thermocapillary drop migration: constant for quasi-steady state? *J. Math. Phys.* **54**, 023102.

YIN, Z., CHANG, L., HU, W. & GAO, P. 2011 Thermocapillary migration and interactions of two nondeformable droplets. *Z. Angew. Math. Mech.* **32**, 761–773.

YIN, Z., CHANG, L., HU, W., LI, Q. & WANG, H. 2012 Numerical simulations on thermocapillary migrations of nondeformable droplets with large Marangoni numbers. *Phys. Fluids* **24**, 092101.

YIN, Z., GAO, P., HU, W. & CHANG, L. 2008 Thermocapillary migration of nondeformable drops. *Phys. Fluids* **20**, 082101.

YOUNG, N., GOLDSTEIN, J. & BLOCK, M. 1959 The motion of bubbles in a vertical temperature gradient. *J. Fluid Mech.* **6**, 350–356.

ZHANG, X. G. & DAVIS, R. H. 1992 The collision rate of small drops undergoing thermocapillary migration. *J. Colloid Interface Sci.* **52**, 548–561.

ZHAO, J., ZHANG, L., LI, Z. & QIN, W. 2011 Topological structure evolvement of flow and temperature fields in deformable drop Marangoni migration in microgravity. *Intl J. Heat Mass Transfer* **54**, 4655–4663.

ZHOU, H. & DAVIS, R. 1996 Axisymmetric thermocapillary migration of two deformable viscous drops. *J. Colloid Interface Sci.* **181**, 60–72.